JOURNAL OF PETROLOGY | VOLUME 47 | NUMBER 1 | PAGES 35–69 | 2006 | doi:10.1093/petrology/egi066

The 26·5 ka Oruanui Eruption, Taupo Volcano, New Zealand: Development, Characteristics and Evacuation of a Large Rhyolitic Magma Body

C. J. N. WILSON[1,2]*, S. BLAKE[3], B. L. A. CHARLIER[3,4] AND A. N. SUTTON[3]

[1]DEPARTMENT OF GEOLOGY, AUCKLAND UNIVERSITY, PRIVATE BAG 92019, AUCKLAND 1020, NEW ZEALAND

[2]INSTITUTE OF GEOLOGICAL & NUCLEAR SCIENCES, PO BOX 30368, LOWER HUTT 6315, NEW ZEALAND

[3]DEPARTMENT OF EARTH SCIENCES, THE OPEN UNIVERSITY, WALTON HALL, MILTON KEYNES MK7 6AA, UK

[4]DEPARTMENT OF EARTH SCIENCES, UNIVERSITY OF DURHAM, DURHAM DH1 3LE, UK

RECEIVED AUGUST 28, 2004; ACCEPTED JUNE 21, 2005
ADVANCE ACCESS PUBLICATION AUGUST 31, 2005

The caldera-forming 26·5 ka Oruanui eruption (Taupo, New Zealand) erupted ~530 km^3 of magma, >99% rhyolitic, <1% mafic. The rhyolite varies from 71·8 to 76·7 wt % SiO_2 and 76 to 112 ppm Rb but is dominantly 74–76 wt % SiO_2. Average rhyolite compositions at each stratigraphic level do not change significantly through the eruption sequence. Oxide geothermometry, phase equilibria and volatile contents imply magma storage at 830–760°C, and 100–200 MPa. Most rhyolite compositional variations are explicable by ~28% crystal fractionation involving the phenocryst and accessory phases (plagioclase, orthopyroxene, hornblende, quartz, magnetite, ilmenite, apatite and zircon). However, scatter in some element concentrations and $^{87}Sr/^{86}Sr$ ratios, and the presence of non-equilibrium crystal compositions imply that mixing of liquids, phenocrysts and inherited crystals was also important in assembling the compositional spectrum of rhyolite. Mafic compositions comprise a tholeiitic group (52·3–63·3 wt % SiO_2) formed by fractionation and crustal contamination of a contaminated tholeiitic basalt, and a calc-alkaline group (56·7–60·5 wt % SiO_2) formed by mixing of a primitive olivine–plagioclase basalt with rhyolitic and tholeiitic mafic magmas. Both mafic groups are distinct from other Taupo Volcanic Zone eruptives of comparable SiO_2 content. Development and destruction by eruption of the Oruanui magma body occurred within ~40 kyr and Oruanui compositions have not been replicated in vigorous younger activity. The Oruanui rhyolite did not form in a single stage of evolution from a more primitive forerunner but by rapid rejuvenation of a longer-lived polygenetic, multi-age 'stockpile' of silicic plutonic components in the Taupo magmatic system.

KEY WORDS: *Taupo Volcanic Zone; Taupo volcano; Oruanui eruption; rhyolite, zoned magma chamber; juvenile mafic compositions; eruption withdrawal systematics*

INTRODUCTION

Large silicic magmatic systems

Large, caldera-forming silicic explosive eruptions provide insights into crustal magmatic processes and represent rare, but catastrophically hazardous, events. Many studies have been made of the associated deposits (principally ignimbrites) and inferences made about the growth of and pre-eruptive conditions in the parental magma bodies (e.g. Smith, 1979; Hildreth, 1981, for reviews). Mostly the caldera-forming eruption is perceived as the culmination of a particular magmatic cycle with a lifetime of the order 10^5–10^6 years (Smith, 1979; Spera & Crisp, 1981; Jellinek & DePaolo, 2003). Snapshots of such systems are also given by pre- and post-climactic volcanism, typically at intervals of 10^4–10^5 years (e.g. Metz & Mahood, 1985,

*Corresponding author. Telephone (+64) 9 373 7599. Fax (+64) 9 373 7435. E-mail: cjn.wilson@auckland.ac.nz

1991; Stix *et al.*, 1988; Halliday *et al.*, 1989; Hildreth *et al.*, 1991; Davies *et al.*, 1994; Davies & Halliday, 1998; Christiansen, 2001). In virtually all examples, the climactic eruptives show systematic variations with respect to one or more of the major and trace elements, crystal contents and isotopic compositions. In such cases, the stratigraphic ordering in the deposit is inverted to obtain the vertical ordering in the chamber (Hildreth, 1981). Such chamber zonations may arise through *in situ* processes (de Silva & Wolff, 1995, for review), or successive emplacement of magma batches of contrasting genesis (e.g. Vogel *et al.*, 1989; Cambray *et al.*, 1995; Mills *et al.*, 1997; Bindeman & Valley, 2003).

A contrast to these 'global' views is offered by Quaternary silicic magmatism in the central Taupo Volcanic Zone (TVZ) of New Zealand, where, within an area of ~120 × 60 km, numerous moderate- to large-scale (~30 to >500 km^3 magma) caldera-forming eruptions have occurred on average every 50 000–100 000 years (Ewart *et al.*, 1975; Houghton *et al.*, 1995; Wilson *et al.*, 1995). The central TVZ is also notable for the high frequency of inter-caldera (in time) and intra-caldera (in space) activity; for example, in the last 65 000 years, there have been at least three caldera-forming events (Rotoiti, Oruanui, Taupo) and ~60 other silicic eruptions (Wilson, 1993, and unpublished data; Jurado-Chichay & Walker, 2000; Nairn, 2002). Thus, regardless of whether a single volcano like Taupo (comparable in size to the Long Valley or Valles calderas) is examined, or the whole central TVZ is considered as one complex system (comparable in size and longevity to the Yellowstone volcanic field), the 'snapshots' afforded by silicic eruptions in New Zealand are given at more frequent intervals than in any comparably sized system worldwide. In addition, although many TVZ rhyolites do show compositional variations (e.g. Briggs *et al.*, 1993; Brown *et al.*, 1998*a*; Beresford *et al.*, 2000; Milner *et al.*, 2003; Nairn *et al.*, 2004), there are two unusual features. First, the variable compositions tend not to be systematically ordered, or are 'reversely' ordered, in the eruption deposits (see Hildreth, 1981). Secondly, some of the variations are such that two or more discrete sources or magma bodies (as opposed to chemically discrete bodies in juxtaposition in a single chamber, e.g. Vogel *et al.*, 1989) have to be invoked in single eruptions.

Here, we document the petrology of the youngest large TVZ caldera-forming event—the 26·5 ka, ~530 km^3 (magma) Oruanui eruption—to illustrate the complexities in TVZ caldera-forming silicic eruptions. The Oruanui is comparable to or larger than events such as the Bishop Tuff and the two members of the Bandelier Tuff, themselves considered to culminate long evolutionary histories. However, the Oruanui was preceded and followed by numerous silicic eruptions within the preceding ~40 000 and following 26 500 years that reflect the rapid accumulation of a large magma body and the post-climactic reorganization of the remaining magma system. The pre-eruptive build-up is summarized here (after Sutton *et al.*, 1995) and more detailed stratigraphic and petrological aspects will be presented elsewhere. This paper documents the Oruanui rhyolitic and mafic magmas, whereas the post-Oruanui deposits have been described by Wilson (1993) and Sutton *et al.* (1995, 2000). The sources and timing of <60 ka rhyolite magma generation at Taupo from zircon geochronology have been considered by Charlier *et al.* (2005).

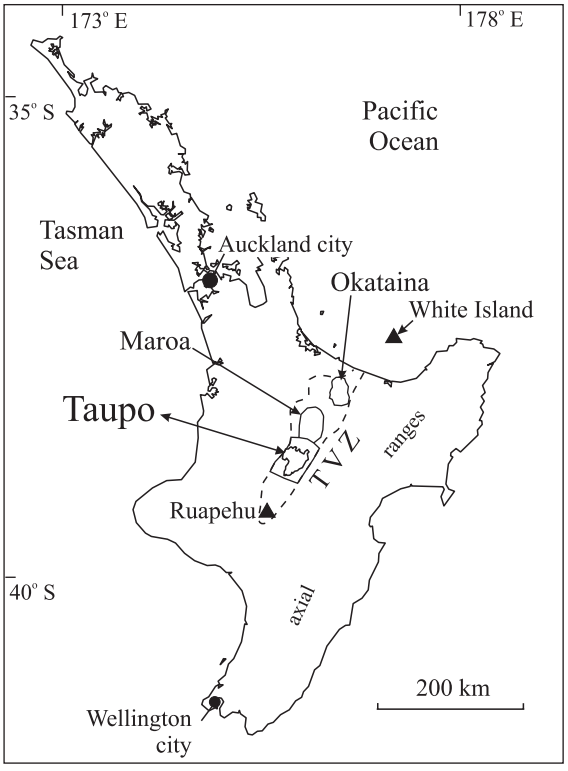

Fig. 1. North Island, New Zealand, showing the Taupo Volcanic Zone (TVZ: dashed outline), and the locations of the main young (<65 ka) rhyolitic volcanoes: Taupo, Maroa (last active at ~17 ka) and Okataina (last active in 1886). Ruapehu and White Island are active andesite/dacite composite cones, data from which are used for comparative purposes in this paper.

Taupo volcano and the lead-up to the Oruanui eruption

Taupo volcano and its northern neighbour, Maroa (Fig. 1), overprint a large caldera associated with the 340–320 ka Whakamaru-group of ignimbrites (Wilson *et al.*, 1986; Houghton *et al.*, 1995). At Taupo, activity in the past ~150 kyr has waxed coevally with the waning of lava-dominated activity at Maroa (Leonard, 2003) and the modern activity of overwhelmingly (>95%) pyroclastic volcanism, from vents mostly now concealed

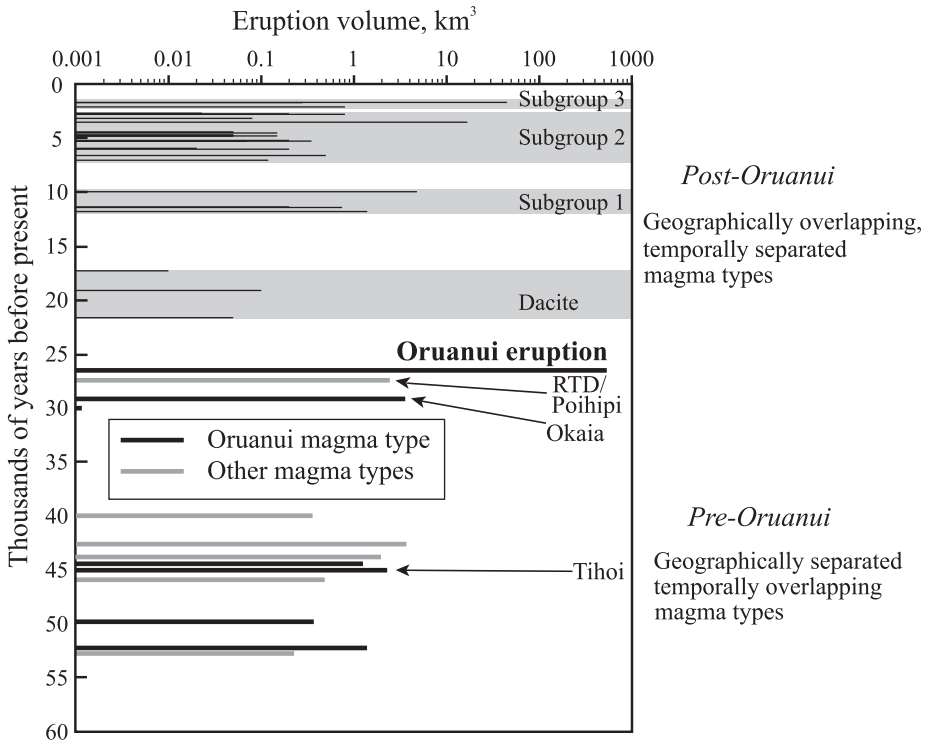

Fig. 2. Time–volume diagram summarizing the eruptive activity and magma systems extant in the Taupo area over the last 60 kyr. Eruptions prior to 30 ka are only roughly dated on the degrees of palaeosol development with respect to age data on other Okataina-derived eruptions. Ages for the Okaia onwards are based on calibrated radiocarbon ages, from Wilson (1993) and Newnham *et al.* (2003). Eruption volumes are approximate magma volumes. Named units are discussed in the text; the shaded zones marked Dacite and Subgroups 1–3 refer to magma groups discussed by Sutton *et al.* (2000). RTD, Rubbish Tip dome.

beneath Lake Taupo, began around 65 ka. Pyroclastic deposits exposed in the Taupo–Maroa area represent 11 eruptions from ~60 to 27·3 ka (CJNW work in progress; see Vucetich & Howorth, 1976), the Oruanui at 26·5 ka (Wilson, 2001), then a sequence of 28 eruptions, all but three of them since 12 ka (Wilson, 1993; Fig. 2).

At Taupo before 65 ka, there were several groupings of silicic eruptives that appear (in the absence of a detailed chronology) to have been geographically confined, such that lavas and pyroclastic deposits erupted in given areas share certain characteristics (Sutton *et al.*, 1995). The largest of these groups forms domes of the Whakaroa ridge immediately north of Lake Taupo (Fig. 3a). They are undated but are constrained to have erupted from ~150 to 60 ka from stratigraphic relationships with dated units. Whakaroa domes have broadly similar compositions to the Oruanui eruptives, with overlap in $^{87}Sr/^{86}Sr$ ratios (Fig. 4) and Fe–Ti oxide temperatures (755–820°C), but differ in being more crystal-rich (8–32%, average 23% ($n = 12$)) and occasionally having phenocrystic biotite (Sutton, 1995).

From ~60 to 26·5 ka, rhyolitic magmas of contrasting compositions were erupted in the Taupo–Maroa area. Some of these eruption deposits have compositions similar to the rhyolite of the Oruanui eruption, are referred to here as being of 'Oruanui type', and are inferred to represent precursor leaks. These alternate with a distinctive composition ('NE dome type' of Sutton *et al.*, 1995) that vented at two sites now marked by Ngangiho (~45 ka), and Rubbish Tip plus Trig 9471 (27·3 ka) domes (Figs 3a and 4). The 'Oruanui type' rhyolites have moderate phenocryst contents (3–13% in the Oruanui itself), hypersthene plus hornblende as the ferromagnesian phases, $^{87}Sr/^{86}Sr$ ratios of 0·70548–0·70568 (Fig. 4) and, for three examples, distinctly bimodal zircon model-age spectra (Charlier *et al.*, 2005). The 'NE dome type' has higher crystal contents (12–24%: Sutton, 1995), biotite as an additional phenocryst phase, lower $^{87}Sr/^{86}Sr$ ratios of 0·70526–0·70530 (Fig. 4) and (for the Rubbish Tip dome) a unimodal zircon age spectrum (Charlier *et al.*, 2005). Known or inferred vent sites for these unrelated rhyolites are as close together as ~14 km (Fig. 3), yet interbedding of their pyroclastic deposits demonstrates that the two magma systems were coeval.

The earliest eruptives of Oruanui-type composition vented just prior to the 62 ± 2 ka Rotoehu Tephra marker horizon (from Okataina volcano: Charlier *et al.*, 2003*a*). Although mineralogically different from other precursory leaks and the Oruanui rhyolites, these earliest

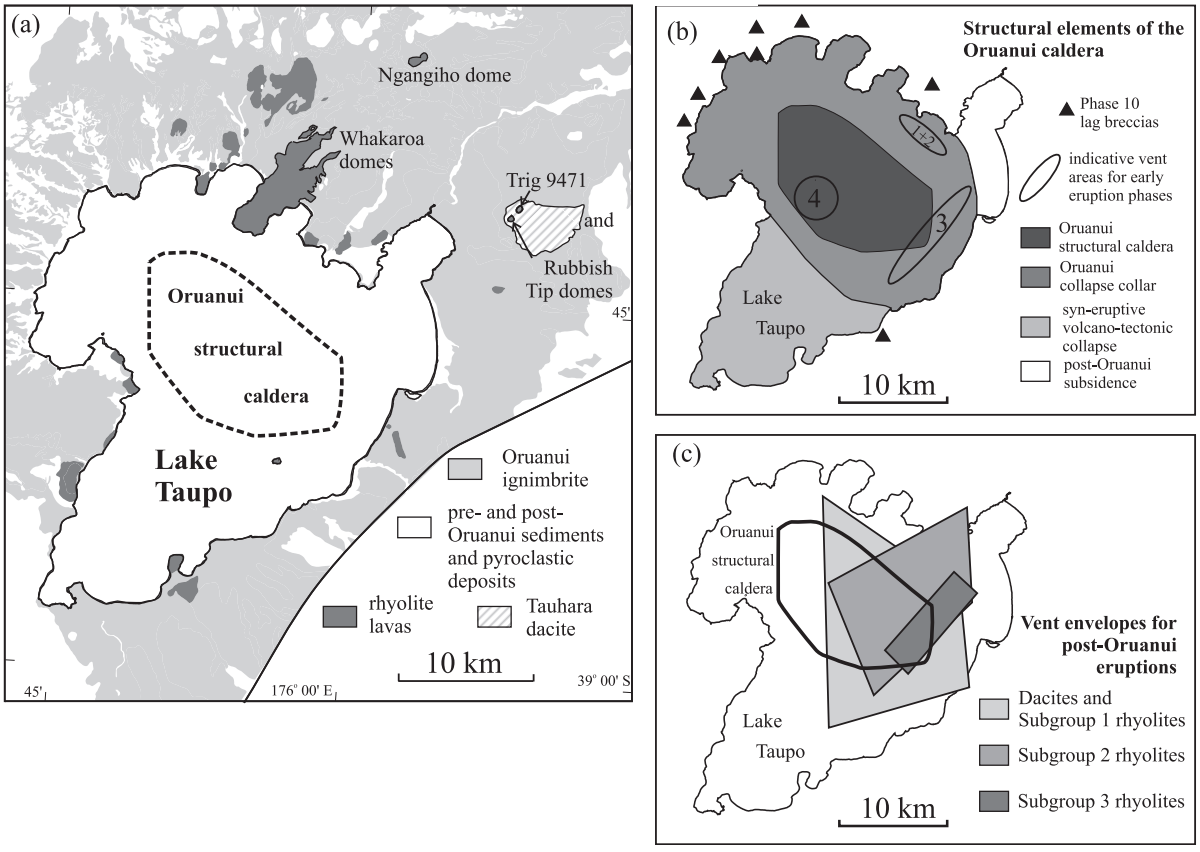

Fig. 3. (a) Simplified geological map of the Lake Taupo area. Labelled rhyolite domes are those discussed in the text. (b) Interpretative structural map (from Wilson, 2001), showing inferred vent areas during the first four of the 10 Oruanui eruption phases and structural elements of the Oruanui caldera. (c) Map of envelopes around the inferred vent sites for post-Oruanui eruptions, superimposed on the Oruanui structural caldera. Vent positions from Wilson (1993); magma groupings from Sutton *et al.* (2000).

deposits have similar isotopic and trace element characteristics to the later Oruanui-type eruptives (Sutton, 1995). They are distinguished from other penecontemporaneous eruptives in the Taupo–Maroa area on the basis of one or more of: crystal content, mineralogy, trace-element geochemistry and Sr-isotopic values (Sutton, 1995). Compositions of the Oruanui-type magma show some variability, but plausibly can be linked by closed-system fractionation involving the phenocrysts present in the rocks (Sutton, 1995). However, as rhyolites that were more- and less-evolved than any precursor leaks were erupted during the climactic eruption, this implies that the evolution of the Oruanui magma batch did not simply involve fractionation of a single body, first established around 65 ka, but that substantial recharge must have occurred at one or more stages. Total volumes of precursor leaks of the Oruanui-type magma amount to only 1–10 km^3 of magma.

After the Oruanui eruption, magmatic systems in the Taupo area apparently were reorganized, with no signals of the earlier compositions being discernible in any mixing trends or overlaps in composition. Post-Oruanui compositions are grouped into four batches (one earliest dacite, three later rhyolite) that are temporally distinct (Fig. 2); however, the vents for these largely overlap spatially, both with each other and with the Oruanui caldera (Sutton *et al.*, 2000; Fig. 3c). The Oruanui event thus marks not only the largest eruption in the TVZ for ~300 kyr, but also a major reorganization of magmatic systems in the Taupo area (Charlier *et al.*, 2005).

THE ORUANUI ERUPTION

The Oruanui eruption (Wilson, 2001) generated 430 km^3 of fall, 320 km^3 of pyroclastic density current (PDC) and 420 km^3 of primary intracaldera deposits, equivalent to ~530 km^3 of magma (of which 300 km^3 is represented by sampleable extra-caldera deposits). The eruption is divided into 10 phases, was spasmodic and in total may have lasted for several months (Table 1; Wilson, 2001). The fall deposits are unusually fine-grained because of magma–water interaction in a precursor Lake Taupo (Self & Sparks, 1978). PDC deposits (entirely non-welded, mostly ignimbrite) were generated throughout the

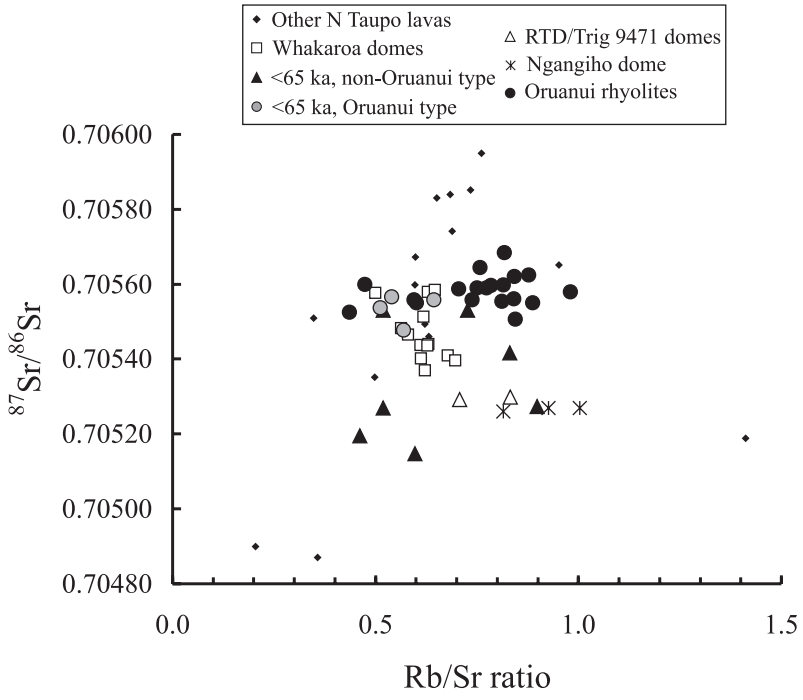

Fig. 4. Summary of the chemical and isotopic relationships between the Oruanui rhyolites and other contemporaneous and earlier eruptives in the north Taupo area. The data marked '<65 ka, Oruanui type' include the Okaia, Tihoi and one other eruption between 65 and 26·5 ka (Fig. 2). The asterisks and open triangles are samples from the 'NE dome type' magma, and the filled triangles show other silicic eruptives from 65 to 26·5 ka.

eruption. They are correlated with eruption phases by interbedding relationships with the fall deposits, and by the presence of three 'spikes' in the abundance of juvenile mafic material (see below). Vent sites appear to have shifted between earlier phases (1–4) of the eruption (Fig. 3b) but, because proximal fall deposits for phases 5–10 are missing (largely because of replacement by coeval ignimbrite), subsequent vent locations are not known. The Oruanui caldera collapse climaxed in phase 10, as evidenced by proximal lithic lag breccias (Fig. 3b), and in this phase, venting of magma may have occurred from sources distributed widely within the northern part of what is now Lake Taupo. The caldera consists of a central 140 km^2 structural collapse area (Davy & Caldwell, 1998) that corresponds to a 'hole' some 2·5–3 km deep, together with a peripheral collapse collar and other areas of inferred syneruptive collapse and faulting (Fig. 3b).

Three factors are important with respect to the petrology of Oruanui eruption products:

(1) Nearly all pyroclasts are white, highly vesicular felsic pumice, with rare 1–10 cm-sized grey to black, poorly vesicular mafic clasts, and rare mingled pumices incorporating both lithologies plus pale grey pumiceous material. The mafic clasts are inferred to be juvenile from the presence of: cauliform or crenulate chilled margins, liquid–liquid contacts between them and local rinds of white pumice, quench crystallization textures and sparse micro-inclusions of vesicular rhyolitic glass. Although rare as lapilli, the mafic clasts also occur as ash in the matrices of fall deposits and ignimbrite, typically to 0·1–0·5 wt %. However, there are three pronounced 'spikes' in concentration (up to 4 wt % of the juvenile fraction) in deposits of phases 3 plus 4, 7 and early 9, which are used to correlate fall deposits and coeval ignimbrite (Wilson, 2001: fig. 3).

(2) Most fall and early PDC deposits are fine-grained (mean grain sizes of 20–60 μm), such that single clasts are not large enough to analyse. Important exceptions are the phases 1 and 2 fall deposits where lapilli- to block-sized clasts are available. For some stratigraphic levels, analyses of multiple 2–4 cm diameter clasts had to be used; such sizes are large enough to minimize crystal losses (Wolff, 1985). On the other hand, much of the later proximal ignimbrite contains clasts of sizes suitable for analysis, but lacks visible markers to place them in their stratigraphic context. Here, correlations between fall deposits and ignimbrite yielded by the juvenile mafic spikes (note (1) above) are used to allocate sampled ignimbrite clasts to their respective eruption phases.

(3) There is little obvious diversity in the properties (e.g. density, crystal content) of the felsic pumices with

Table 1: Summary stratigraphy of the deposits and timing of the Oruanui eruption

Phase	Nature of deposits	Fall deposit bulk volume	PDC deposit bulk volume (O.M.)
1	Single pumice fall unit, accompanied by moist to wet low-velocity PDCs to northwest of vent	0·8	0·01
	Time break of several weeks to months		
2	Three pumice fall beds interspersed with proximal PDC material, pumiceous fine ash, or phase-3-like very fine ash	0·8	0·1
	Continuous activity, no time break		
3	Wet-erupted unit; proximal mixed PDC and fall deposits, distal multiple-bedded fall material	>5	10
	Continuous activity, no time break		
4	Single pumice fall bed with interbedded thin but widespread PDC deposit	2·5	0·1
	Time break of hours		
5	Single pumice fall bed with only minor coeval PDC deposits	14	1
	Time break of hours to days		
6	Mixed dry- and wet-erupted fall units, accompanied by widespread multiple PDC deposits	5·5	10
	Time break of hours		
7	Single pumice fall bed, accompanied by widespread and voluminous PDC deposits	15	10
	Continuous activity, no time break		
8	Wet-erupted fall deposit, rich in accretionary lapilli, accompanied by voluminous and most widespread PDC deposits	37	10
	Continuous activity, no time break		
9	Single ash and pumice fall bed, accompanied by voluminous PDC deposits, but deposition mainly in proximal areas	85	10
	Time break of hours to days		
10	Fine-grained ash-fall beds, accompanied by voluminous PDC deposits that are confined to areas around the Lake Taupo basin	~265	100
	Total volumes (km^3)	*430*	*320*

Bulk volumes in km^3 for the pyroclastic density current (PDC) deposits are order-of-magnitude (O.M.) minimum estimates only. See Wilson (2001) for further details.

stratigraphic position. Thus, unlike in (for example) the Bishop Tuff (Hildreth, 1979), it is not possible to select clasts on the basis of a visible feature, such as crystal content, in confidence that the full diversity of chemical compositions is being covered. Instead, we collected suites of suitable clasts at stratigraphic levels where their sizes and abundances were optimal, and then saw what compositional diversity was apparent.

ANALYTICAL TECHNIQUES

Pumices 5–40 cm across and mafic clasts >3 cm across were used for individual analyses. Clasts were washed in deionized water to remove adhering matrix, and dried in an oven at 110°C for several days prior to crushing. Clasts were crushed to chips in a hardened steel jaw crusher and then, after screening to remove any weathered pieces, reduced to powder in an agate Tema.

Major and trace elements were determined on this powder using an ARL 8420+ wavelength dispersive XRF spectrometer at the Open University, following the techniques of Ramsey *et al.* (1995). Approximate 2 SD analytical precisions (relative %) found by replicate analyses of the same disc for elements at concentrations typical in the rhyolites are: SiO_2 ± 0·2, TiO_2 ± 2, Al_2O_3 ± 0·3, Fe_2O_3 ± 0·3, MnO ± 3, MgO ± 2, CaO ± 1, Na_2O ± 1, K_2O ± 0·6, P_2O_5 ± 6, Rb ± 1·5, Sr ± 1·5, Y ± 5, Zr ± 1·5, Nb ± 15, Ba ± 3·5, Pb ± 20, Zn ± 3·5, Ga ± 10. Samples were also analysed for selected REE, U, Th, Cs, Ta, Hf, Sc and Co by INAA using the methods of Potts *et al.* (1985). For INAA, 2 SD precisions (relative %) are approximately: REE, Th, Hf ± 5; Ta ± 10; Cs, U ± 15; Sc, Co ± 6. Samples for Sr and Nd isotopic analysis were dissolved in HNO_3 and HF, followed by HCl. Sr and Nd were separated by standard ion exchange techniques and loaded on single Ta and double Re–Ta filaments, respectively. All Sr

measurements were made on a Finnegan MAT 261 multi-collector mass spectrometer in static mode and normalized to $^{86}Sr/^{88}Sr = 0{\cdot}1194$. Sr isotope ratios were determined in three analytical sessions over several years, during which time the average value for NBS 987 showed significant variation (0·710220–0·710255), although the external errors within each session never exceeded 22 ppm (1 SD). Thus, to ensure internal consistency of this dataset, all $^{87}Sr/^{86}Sr$ values have been normalized to the mean value of NBS 987 = 0·71025. Early Nd analyses were performed on the MAT 261, and replicate analyses of an OU J&M Nd standard gave $^{143}Nd/^{144}Nd = 0{\cdot}511780 \pm 28$ (1 SD, $n = 64$). Later analyses were run on a Finnegan MAT 262 with the J&M Nd standard giving $^{143}Nd/^{144}Nd = 0{\cdot}511800 \pm 11$ (1 SD, $n = 40$). All Nd analyses were normalized to $^{146}Nd/^{144}Nd = 0{\cdot}7219$. Blanks for both elements were negligible compared with sample amounts loaded.

Mineral compositions were analysed on a wavelength-dispersive Cambridge Instruments M9 electron microprobe and are subject to 2σ errors of no more than 0·2%, except for Si (0·5%), as determined by replicate analyses of a basaltic glass standard. During analysis of Fe–Ti oxides, rutile (99·3% TiO_2) was analysed as a secondary standard in order to minimize errors because of drift in Ti calibration.

ORUANUI JUVENILE COMPOSITIONS

Juvenile clasts are of three types: white felsic pumices, dark grey mafic to intermediate scoriae (basaltic andesite to high-Si andesite, referred to as mafic clasts in this paper), and streaky pumices. There is a gap in the composition of homogeneous samples between ~63% (dark grey) and 72 wt % SiO_2 (white); only streaky pumices lie within this gap. The felsic pumices are all rhyolitic and make up over 99% of the juvenile fraction by weight. Because the juvenile clasts within the individual mafic and rhyolitic compositional fields are of similar appearance in hand specimen, their compositions are described first, then the petrographic and mineralogical characteristics are described for representative clasts from the range of chemical compositions found.

Rhyolites

Whole-rock compositions

Rhyolite pumices from all stratigraphic levels have been analysed; representative data are given in Table 2, and the full dataset is available as Electronic Appendix 1 on the *Journal of Petrology* website at http://www.petrology.oupjournals.org. All analysed pumices reported here are secondarily hydrated, but have clear glass, and no traces of clay alteration, leaching or enrichment, with the possible exception of Na_2O.

The pumices show significant variations in major and trace elements (e.g. SiO_2: 71·8–76·7 wt %; K_2O: 2·45–3·13 wt %; Rb: 76–112 ppm, Zr: 282–128 ppm); however, there is a dense clustering of data in a relatively restricted compositional range, with fewer samples trending towards somewhat more- and markedly less-evolved compositions ('less-evolved' hereafter refers specifically to pumices with <73·8 wt % SiO_2). Of the three Oruanui rhyolite compositional groups reported by Sutton (1995) and Sutton *et al.* (1995), one ('HKRR') is now recognized by us as coming from deposits that represent a different, older eruption, and the boundary between the less-evolved 'LKRRp' and dominant, more-evolved 'LKRRe' groups corresponds to our 73·8% SiO_2 value. In plots of major elements against SiO_2 (Fig. 5), most oxides show coherent trends, except that MgO, Na_2O and P_2O_5 show some scatter. In plots of trace elements (Fig. 6), Rb and Ba behave incompatibly, whereas Sr, Zn and Zr behave compatibly. Much of the scatter in Figs 5 and 6 reflects the compositions of 18 samples that have unusually high MgO for their SiO_2 content (Fig. 5e) and/or unusually low SiO_2 for their Zr content (Fig. 6d). These samples, hereafter referred to as 'high-Mg rhyolites', are discussed further in the section on 'Origins of Variations in the Oruanui Magmas'.

Four rhyolite samples have been further analysed by INAA (Table 3). With increasing silica, U, Th and Cs behave incompatibly, Hf behaves similarly to Zr and decreases markedly, the LREE remain approximately constant, and the MREE and HREE are depleted, following the behaviour of Y. All samples are LREE-enriched ($Ce_N/Yb_N = 4$–5), have flat HREE profiles, and modest negative Eu anomalies (Fig. 7a). The Oruanui rhyolites have a restricted range of $^{87}Sr/^{86}Sr$ (0·70550–0·70568) and $^{143}Nd/^{144}Nd$ values (0·512613–0·512815) when compared with the ranges shown by older rhyolites around Taupo volcano (Figs 4 and 8a). However, in detail, variations in $^{87}Sr/^{86}Sr$ ratios (Fig. 9) exceed analytical errors.

Petrography and mineral chemistry

Phenocryst contents have been measured by panning methods and from the ratios of Rb and K in glass to whole-rock, yielding 3–13% crystallinity (Table 4). Phenocryst contents decrease slightly with increasing SiO_2. All rhyolite pumices contain the phenocryst assemblage plagioclase + orthopyroxene + quartz + hornblende + magnetite + ilmenite, together with apatite and zircon as accessory minerals. All work on Oruanui rhyolite pumices reported here was performed on crystal separates rather than thin sections, so point-counting has not been performed. Estimates of mineral proportions were made for samples for which glass analyses

Table 2: Representative analyses of Oruanui rhyolites and glass separates

Sample:	P915	P1042	P1181	P1291	P740	P1294	P1322A	P1320A	P1208	P695	P1322C	P1319	P1209	P1322B	P1335
Phase:	3	6	3	3	6	6	3	3	10	7	3	1	10	3	1
Type:	Single	Single	Single	Multiple	Single	Multiple	Single	Single	Single	Single	Single	Single	Single	Single	Single
SiO_2	71·79	71·86	72·30	73·01	73·76	74·15	74·71	74·73	74·89	74·93	75·57	75·63	75·72	75·89	75·95
TiO_2	0·42	0·40	0·40	0·36	0·29	0·25	0·25	0·25	0·24	0·24	0·23	0·23	0·21	0·21	0·21
Al_2O_3	14·69	14·53	14·73	14·99	14·34	14·24	13·68	13·63	13·64	13·55	13·08	13·13	13·06	13·04	13·13
Fe_2O_3	3·05	2·96	2·93	2·73	2·34	2·12	2·21	2·21	2·00	1·94	2·08	1·87	1·74	1·83	1·74
MnO	0·10	0·10	0·09	0·08	0·07	0·07	0·06	0·06	0·06	0·06	0·06	0·07	0·06	0·06	0·06
MgO	0·63	0·65	0·65	0·51	0·41	0·32	0·51	0·52	0·31	0·32	0·45	0·30	0·25	0·34	0·25
CaO	2·53	2·57	2·42	1·96	2·00	1·90	1·88	1·82	1·90	1·87	1·74	1·80	1·70	1·66	1·70
Na_2O	4·15	4·32	3·95	3·83	4·10	4·17	3·71	3·77	4·08	4·01	3·66	4·14	4·32	3·91	4·03
K_2O	2·55	2·51	2·45	2·50	2·64	2·72	2·94	2·95	2·83	3·04	3·09	2·81	2·90	3·03	2·91
P_2O_5	0·09	0·10	0·08	0·04	0·05	0·05	0·04	0·05	0·04	0·04	0·04	0·04	0·04	0·04	0·02
(LOI)	4·49	3·63	3·90	4·77	3·84	3·68	3·95	4·08	3·16	2·63	4·53	3·52	3·53	3·83	3·00
(Total)	98·61	97·00	98·93	99·36	99·37	100·02	99·72	100·00	99·11	99·00	100·39	99·90	99·82	100·11	99·50
Rb	76	80	83	85	92	93	99	100	100	98	102	99	101	102	102
Sr	175	171	175	142	139	131	126	122	134	129	117	128	120	115	121
Y	27	26	26	26	24	24	22	23	24	23	23	23	23	23	23
Zr	282	238	246	230	203	183	137	146	169	160	137	168	147	137	154
Nb	7	7	7	7	7	7	7	6	6	7	6	6	7	7	6
Ba	510	511	517	590	595	608	582	584	593	575	591	582	581	590	594
Pb	11	11	11	12	11	13	11	12	11	13	12	12	13	14	13
Zn	58	53	54	51	48	45	42	43	40	39	40	40	40	38	38
Ga	14	14	15	14	14	15	14	13	12	12	12	12	12	13	13
$^{87}Sr/^{86}Sr$	0·70553		0·70560	0·70555		0·70557		0·70567	0·70558	0·70563		0·70559	0·70551		0·70556
$^{143}Nd/^{144}Nd$	0·512694			0·512615		0·512593		0·512604	0·512626	0·512738			0·512613		0·512626
ε_{Nd}	1·09			−0·45		−0·88		−0·66	−0·23	1·95			−0·49		−0·24

Sample:	P1039	P894	P888	P915glass	P1294glass	P1209glass	P1039glass	P888glass
Phase:	6	10	10	3	6	10	6	10
Type:	Single	Single	Single	Glass	Glass	Glass	Glass	Glass
SiO_2	76·02	76·43	76·66	73·43	76·33	76·91	77·02	77·21
TiO_2	0·20	0·18	0·18	0·35	0·19	0·16	0·16	0·16
Al_2O_3	13·01	12·90	12·75	14·07	13·21	12·65	12·59	12·51
Fe_2O_3	1·66	1·54	1·55	2·52	1·59	1·43	1·40	1·36
MnO	0·06	0·05	0·05	0·09	0·06	0·05	0·05	0·05
MgO	0·25	0·21	0·19	0·40	0·16	0·17	0·16	0·14
CaO	1·62	1·51	1·42	2·07	1·40	1·31	1·32	1·26
Na_2O	4·17	4·06	4·03	4·31	4·03	4·13	4·14	4·04
K_2O	2·97	3·08	3·13	2·68	3·01	3·16	3·14	3·24
P_2O_5	0·04	0·03	0·03	0·09	0·03	0·03	0·03	0·02
(LOI)	3·12	3·09	3·19	5·09	3·97	3·29	3·46	3·49
(Total)	100·01	99·70	99·23	99·98	99·73	99·26	99·89	100·75
Rb	104	106	106		101	112	109	112
Sr	118	108	102		99	94	96	91
Y	24	23	23		24	24	24	24

Sample:	P1039	P894	P888	P915glass	P1294glass	P1209glass	P1039glass	P888glass
Phase:	6	10	10	3	6	10	6	10
Type:	Single	Single	Single	Glass	Glass	Glass	Glass	Glass
Zr	146	138	133		158	136	137	128
Nb	6	6	6		7	7	7	7
Ba	600	604	602		606	616	613	623
Pb	12	12	13		13	12	13	13
Zn	37	36	37		42	40	37	39
Ga	13	11	12		12	12	12	13
$^{87}Sr/^{86}Sr$		0·70558						
$^{143}Nd/^{144}Nd$		0·512682						
ε_{Nd}		0·85						

'Type' denotes whether single or multiple pumices were used, or a glass separate. Oxide data are normalized to 100% volatile free, but the original LOI values and analytical totals are also given.

were available, using a least-squares mass balance technique (Table 4).

Plagioclase forms subhedral, often broken phenocrysts up to 2 mm long that are generally weakly zoned. Up to 5 wt % of the feldspars in the 2 and 1 mm sieve size fractions have cloudy grey cores. Orthopyroxene occurs as subhedral to euhedral prisms up to 2 mm, though more commonly 0·5–1 mm, in length. Quartz forms euhedral to subhedral phenocrysts up to 2 mm in diameter. Hornblende forms euhedral laths, typically 1 mm long, although smaller in the samples in which it is a rare phase. The relative abundance of hornblende correlates inversely with the degree of evolution: the lowest-SiO_2 pumices have hornblende as the dominant ferromagnesian phase; the most abundant rhyolite compositions (74–76 wt % SiO_2) have roughly equal amounts of hornblende and orthopyroxene, and the most evolved samples have orthopyroxene dominant (Table 4). Magnetite often occurs as inclusions in, or attached to, the rims of orthopyroxene (and more rarely in plagioclase and hornblende), though it is also found as discrete microphenocrysts of 0·1–0·25 mm diameter. Ilmenite is less common than magnetite but has a similar mode of occurrence. Apatite occurs as needles, occasionally up to 0·5 mm but typically <0·1 mm in length, mainly in orthopyroxene but also in plagioclase and magnetite. Zircon occurs as inclusions in orthopyroxene, but both it and apatite also occur as free crystals in the glass matrix.

Phenocrysts from 12 rhyolite samples (including two examples of high-Mg clasts), selected to reflect the full range of SiO_2 content and stratigraphic position, have been analysed by electron microprobe. The full dataset is given in Electronic Appendix 2 (available at http://www.petrology.oupjournals.org). Excluding the grey cored crystals, plagioclase ranges continuously from An_{54} to An_{32} and $Or_{0.7}$ to Or_2, with FeO_t decreasing from ~0·4 to 0·2 wt % (Fig. 10a and b). The outer parts of crystals have An contents of <45%. Plagioclase compositions do not correlate with whole-rock composition (Fig. 11a). Zoning in the grey cored plagioclases is much more pronounced, with cores having up to 80% An, although most are only as anorthitic as 70%. Orthopyroxene forms a tight compositional cluster around $En_{55–45}Wo_{1·4–2·6}$, with a small tail extending to $En_{60}Wo_{2·6}$ (Fig. 10c). The ratio En/(En + Fs) does not correlate with whole-rock composition (Fig. 11b). Concentrations of Al_2O_3 (0·2–1·1 wt %) and TiO_2 (0·07–0·21 wt %) are correlated but do not vary systematically with En content. Calcic amphibole ('hornblende') plots in the fields of tschermakite and magnesiohornblende (Leake *et al.*, 1997), with strong positive correlations between $(Na + K)^A$, Ti and Al^T (Fig. 10d), all of which decrease with whole-rock silica (e.g. Fig. 11c). $Mg/(Mg + Fe^{2+})$ and Ca are 0·724 ± 0·041 and 1·674 ± 0·037, respectively (± values are 1 SD, for 32 analyses). Magnetite falls in the range $Usp_{28–35}$ and variation in the minor elements is dominated by Mg and Al, with a strong clustering around 0·46–0·58 Al and 0·21–0·30 Mg atoms per 32 oxygens (Fig. 10e). Most members of this cluster are found in pumice with >73 wt % silica and are similar to the field of magnetite compositions found by Shane (1998); the scattered array of magnetites with higher Mg and Al are found in pumices with <73 wt % SiO_2 (Fig. 11d). Ilmenite is in the range Ilm_{87-92}, with a few scattered to lower values. X_{Ilm} increases and Mg decreases with increasing whole-rock silica (Figs 10f and 11e).

Intensive parameters and water content

Pre-eruptive Fe–Ti oxide equilibration temperatures and oxygen fugacities were calculated by the method of Ghiorso & Sack (1991), which carries an absolute uncertainty in temperature of about ±30°C, and the results are

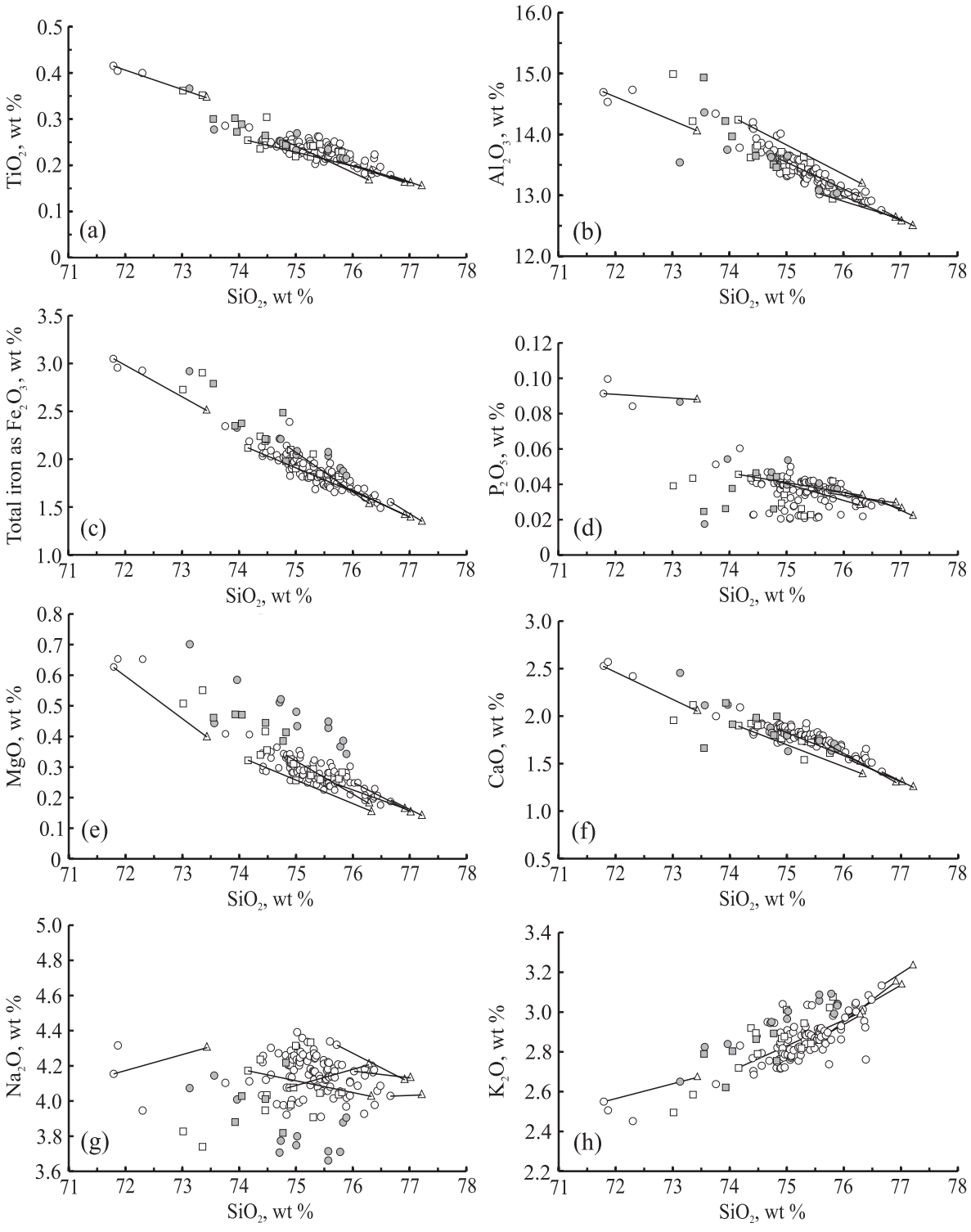

Fig. 5. Plots of selected major oxides against silica for all analysed Oruanui rhyolites. Open symbols denote normal rhyolite, filled symbols denote the high-Mg rhyolite samples (see text). Circles, single pumices; squares, multiple pumices; triangles, glass separates, with tie-lines connecting whole-rock–glass pairs (Table 2).

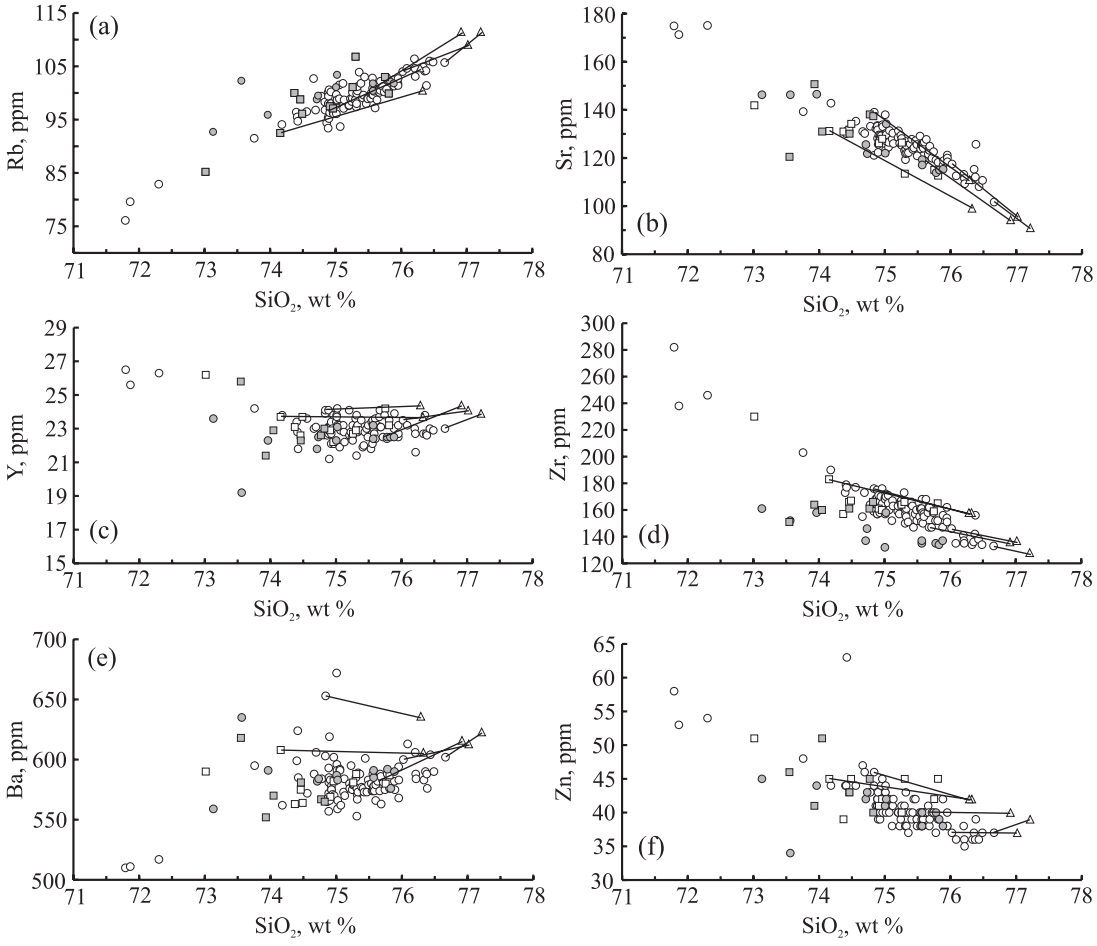

Fig. 6. Plots of selected trace elements for all analysed Oruanui rhyolites. Symbols and tie-lines as in Fig. 5.

Table 3: INAA data from selected Oruanui rhyolites

Sample:	P915	P1291	P1208	P1209
Phase:	3	3	10	10
SiO_2:	71·79	73·01	74·89	75·72
La	20·6	22·3	21·1	20·4
Ce	42·5	45·6	42·8	43·3
Nd	21·8	19·2	17·7	18·1
Sm	4·4	4·0	3·8	3·6
Eu	1·2	0·93	0·79	0·72
Tb	0·78	0·65	0·60	0·60
Yb	3·1	2·3	2·6	2·4
Lu	0·50	0·43	0·42	0·40
Th	8·7	9·4	9·8	10·3
U	1·7	2·5	2·3	2·7
Ta	0·59	0·57	0·56	0·56
Hf	7·0	5·8	4·8	4·2
Cs	3·9	5·7	4·8	4·9
Co	2·1	5·0	1·4	1·2
Cr	5	9	5	4
Sc	10·2	10·3	6·2	5·3

shown in Fig. 12a. Temperatures calculated for eight evolved rhyolite samples with equilibrium oxide pairs (as defined by Bacon & Hirschmann, 1988) overlap within error at 750–770°C. The oxide crystals used have narrow compositional ranges, as described in the previous subsection, and many occur as inclusions within orthopyroxene crystals whose compositions were typical of those in evolved rhyolite. Although oxide pairs were not seen in physical contact, their occurrence and composition indicate that they were in chemical equilibrium and will, therefore, give a meaningful estimate of the evolved rhyolite's temperature prior to eruption. The eight samples also span the stratigraphic range of the deposits, implying that the dominant volume of the erupted magma body had little or no thermal variation. Calculated $\log fO_2$ values are −14·5 to −15·25, and the T–fO_2 data are typical of hornblende-bearing rhyolites in the TVZ and in general (Ewart *et al.*, 1975; Ghiorso & Sack, 1991; Shane, 1998). Hornblende–plagioclase thermometry (Holland & Blundy, 1994) on rim compositions from evolved rhyolite samples yields temperatures in

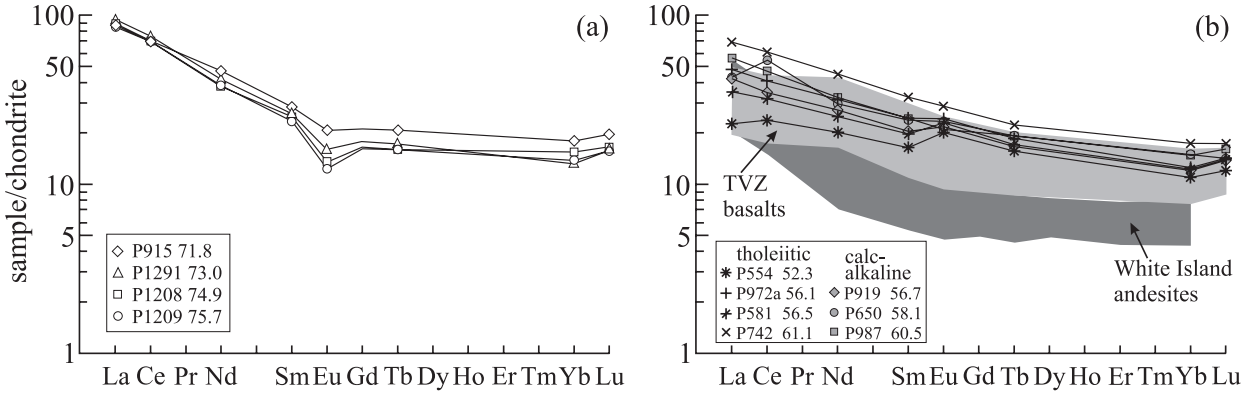

Fig. 7. REE data for (a) normal rhyolitic and (b) mafic Oruanui compositions. Samples used are labelled, together with their SiO_2 percentages and (for mafic samples) their designation into the tholeiitic or calc-alkaline compositional groups (see Tables 3 and 5 for original data). Normalizing values for C1 chondrite are from Sun & McDonough (1989). In (b), the field for TVZ basalts (48·5–53·2 wt % SiO_2) is from Gamble *et al.* (1993*a*, modified with Sun & McDonough normalizing values), and for White Island andesites (55·9–63·3 wt % SiO_2) from Cole *et al.* (2000).

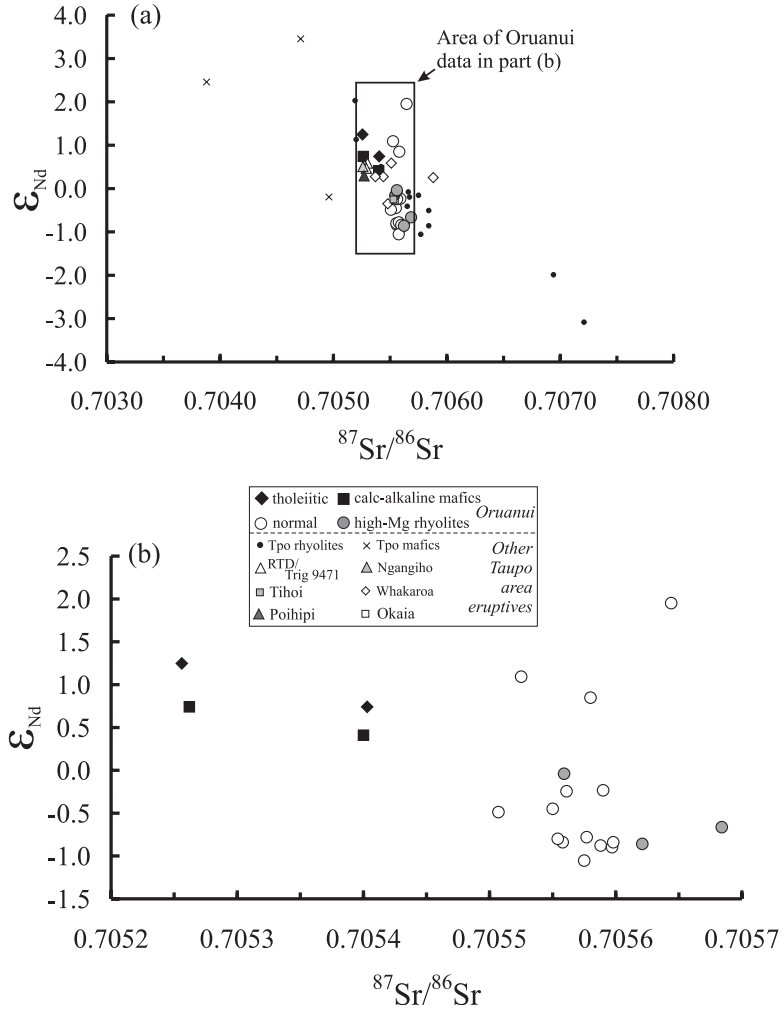

Fig. 8. Plots of $^{87}Sr/^{86}Sr$ versus ε_{Nd} values for rhyolites at Taupo volcano. (a) All data. The symbols for 'Tpo mafics' and 'Tpo rhyolites' represent pre-65 ka eruptives that are inferred to be unrelated to the Oruanui and its precursors. Other pre-Oruanui eruptive units are as discussed in the text and Figs 2 and 4. (b) Enlargement of data from the Oruanui mafic types (tholeiitic, calc-alkaline) and rhyolite.

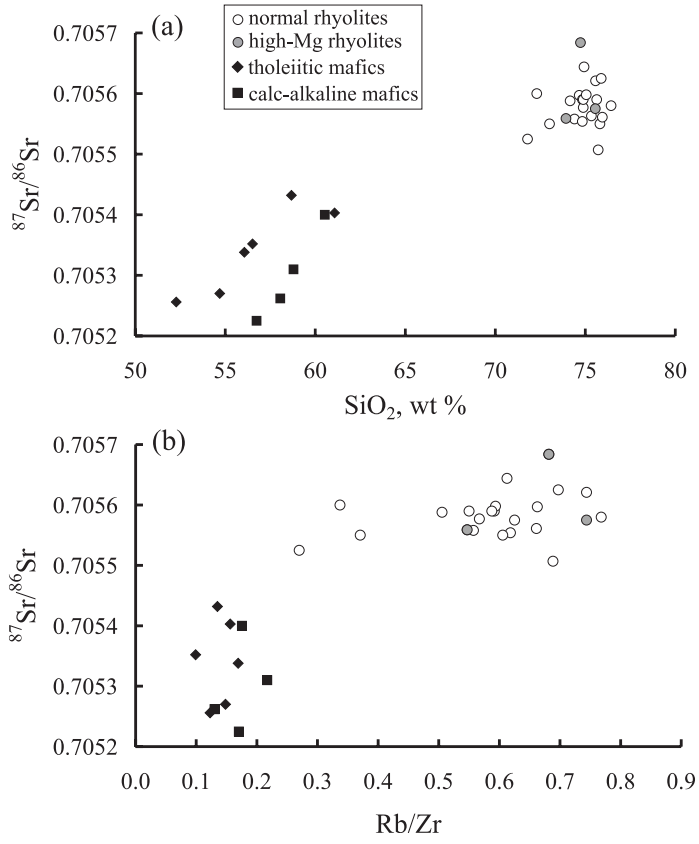

Fig. 9. Plot of $^{87}Sr/^{86}Sr$ ratios versus two indices of differentiation. See text for discussion.

Table 4: Crystallinities and phenocryst assemblages of selected pumices from Oruanui rhyolites

Sample	W.R.	Wt % crystals			Opx:Hb	Glass	Plag	Qtz	Opx	Hb	Mag	Ilm	Ap	Σr^2
	SiO_2	(a)	(b)	(c)										
P915	71·8			6·0	29:71	0·94	0·04	0	0·005	0·011	0·003	0·0007	0·0003	0·12
							66·7	0	8·3	18·3	5·0	1·2	0·5	
P740	73·8	13			42:58									
P1294	74·2	11	10	9·8	45:55	0·90	0·073	0·0085	0·007	0·005	0·006	0·0003	0·0002	0·16
							73·0	8·5	7·0	5·0	6·0	0·3	0·2	
P1322A	74·7	9			59:41									
P1320A	74·7	10			55:45									
P1319	75·6	13			61:39									
P1209	75·7	11	9	10	65:35	0·90	0·064	0·0212	0·007	0·005	0·0019	0·0008	0·0001	0·14
							64·0	21·2	7·0	5·0	1·9	0·8	0·1	
P1039	76·0	7	3·3	6·4	75:25	0·94	0·0415	0·009	0·0045	0·002	0·0022	0·0005	0·0003	0·02
							69·2	15·0	7·5	3·3	3·7	0·8	0·5	
P888	76·7	6	5·2	4·0	82:18	0·96	0·0277	0·007	0·0031	0·00005	0·0015	0·0002	0·0001	0·02
							69·3	17·5	7·8	1·3	3·7	0·5	0·1	

Wt % crystals expressed as measured by (a) panning methods, (b) Rb (whole-rock−glass) methods, and (c) K_2O (whole-rock−glass) methods. Opx:Hb ratio based on counting 100 crystals in a 125−250 μm crystal separate. Crystal assemblages calculated by least-squares methods using glass, phenocryst and whole-rock compositions. All data are from Sutton (1995).

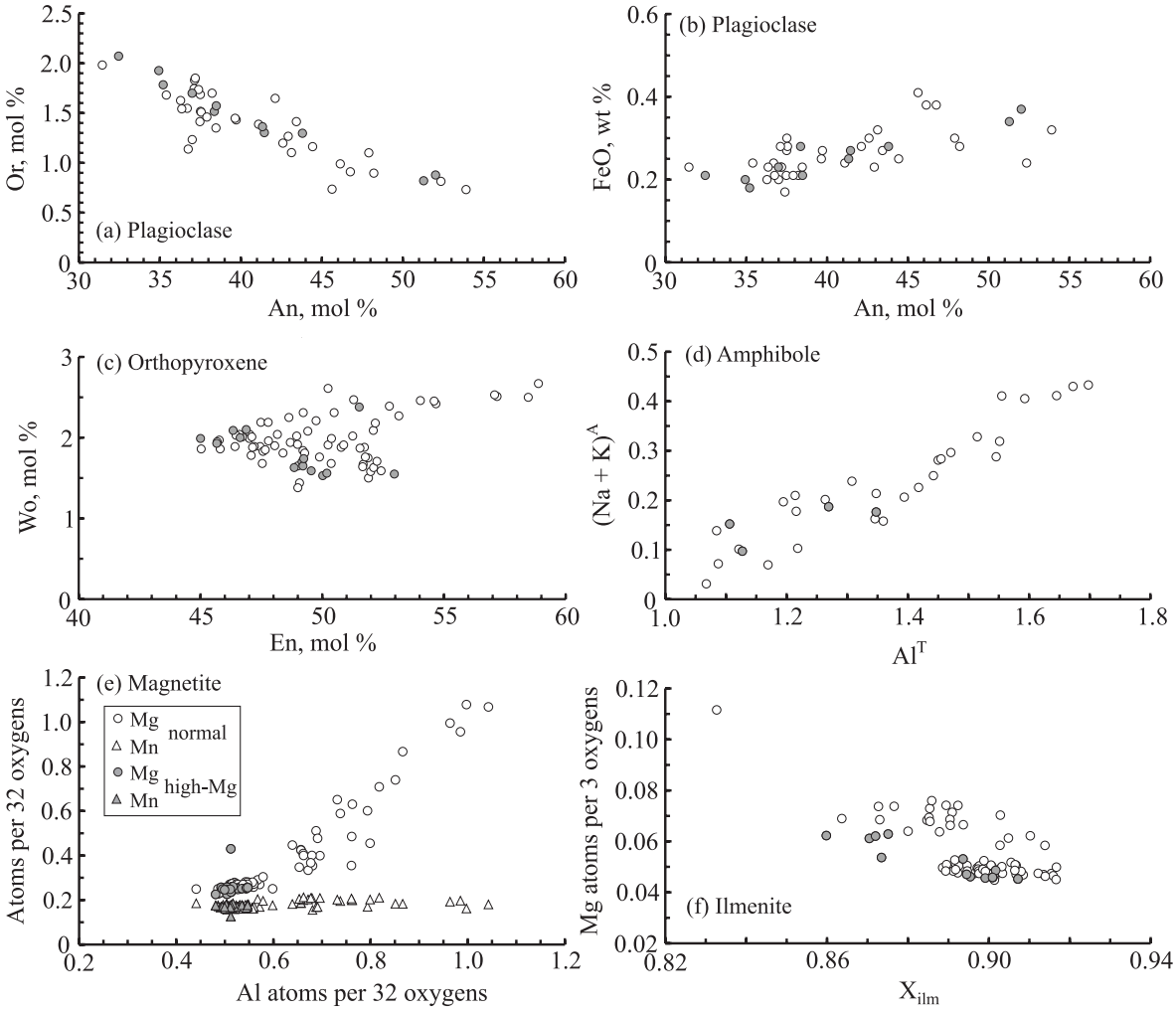

Fig. 10. Plots of mineral compositions in rhyolite pumices. Open and filled symbols denote normal and high-Mg rhyolites, respectively (Fig. 5). See text for discussion.

reasonable agreement with the Fe–Ti oxide temperatures, with a mean of around 800°C, and only two hornblende rims (from P740: 73·8 wt % SiO_2) yielding higher temperatures (800–850°C). Zircon saturation temperatures of glass compositions in the evolved rhyolite, calculated by the method of Watson & Harrison (1983), are above but within error of the Fe–Ti oxide temperatures, consistent with U–Th chronometric evidence for active crystallization of zircon up to the time of eruption (Charlier & Zellmer, 2000; Charlier *et al.*, 2005).

Estimation of temperatures for the less-evolved rhyolite samples (Fig. 12b) is complicated by large ranges in magnetite and ilmenite compositions in some samples, and a lack of equilibrium pairs in others. Equilibrium oxide pairs in P915 yield $T = 815$°C, $\log fO_2 = -13{\cdot}5$. For low Mg/Mn pairs from P1042, a temperature of 820°C and a $\log fO_2 = -13{\cdot}35$ were obtained. In P1181, only one magnetite crystal with relatively low MgO/MnO (1·17) was in Mg/Mn equilibrium with the ilmenites (MgO/MnO = 1·47–1·73); these pairings yield between 820 and 847°C and $\log fO_2 = -12{\cdot}8$ to $-13{\cdot}5$ (mean 830°C, $-13{\cdot}2$). Hornblende–plagioclase thermometry on P915 and P1181 yields temperatures consistently around 840–850°C, within error of the Fe–Ti oxide temperature estimates for these samples, and significantly higher than those obtained for the evolved rhyolite.

Plotting oxide temperatures against glass compositions (Fig. 12c) shows that the liquidus decreases with compositional evolution, as should be expected. Oruanui rhyolite liquidus temperatures at given CaO values are ~70°C lower than the liquidus of the post-Oruanui compositions, consistent with there being no direct petrogenetic link between the two (Sutton *et al.*, 1995, 2000). Qualitatively, the lower liquidus and presence of hornblende in

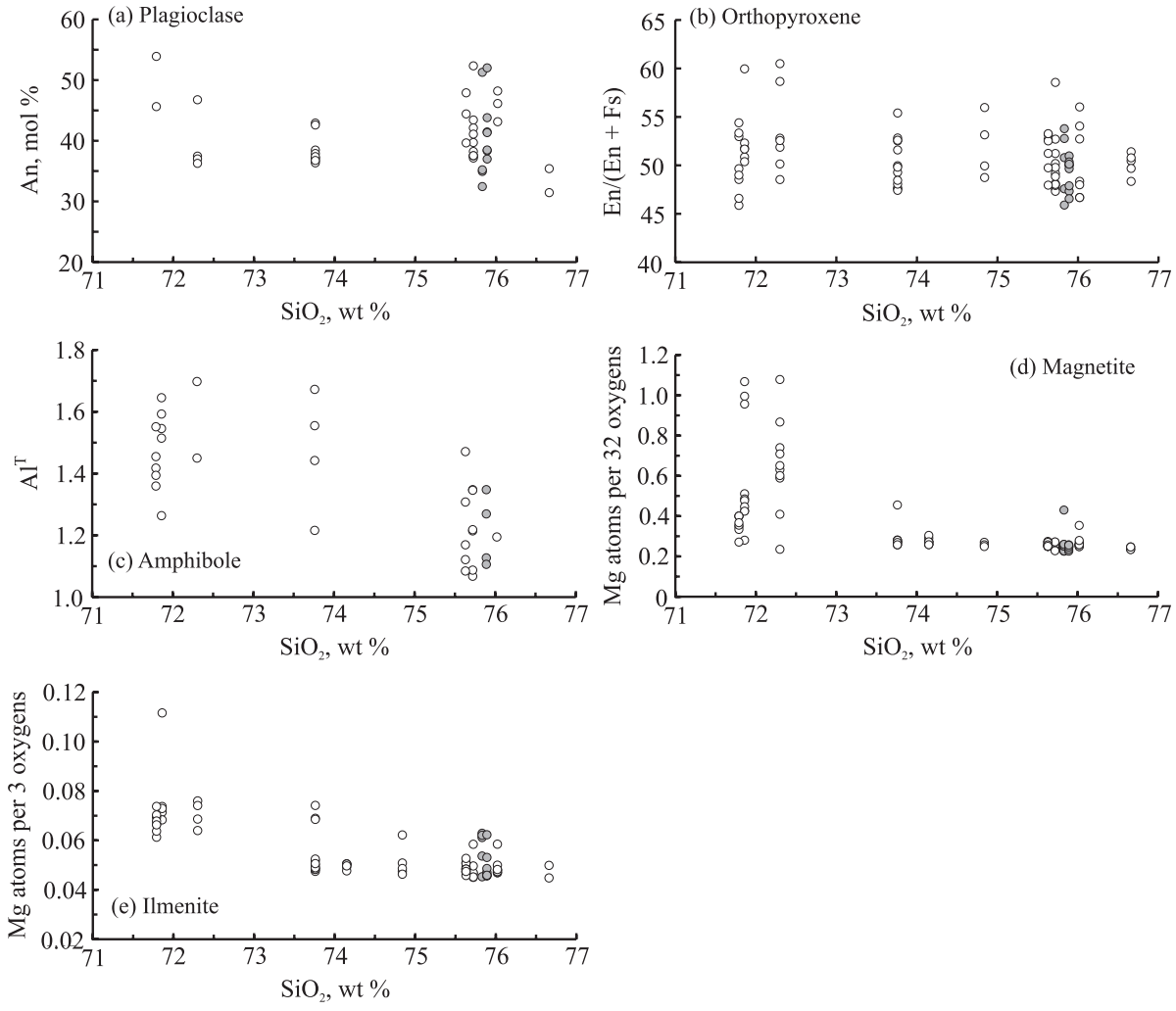

Fig. 11. Plots of mineral composition in Oruanui rhyolites versus the composition of their host pumice. Open and filled symbols denote normal and high-MgO rhyolites, respectively (Fig. 5). See text for discussion.

the Oruanui rhyolite suggest that this magma experienced higher water pressures than the post-Oruanui rhyolite. Comparing the rhyolite liquidi with experimental results on water-saturated liquids of similar composition (in terms of SiO_2, CaO and Na_2O/K_2O) with the Taupo rhyolites shows that the post-Oruanui compositions imply equilibration from 100 to 200 MPa water pressure, whereas the Oruanui magmas exceeded 200 MPa (Fig. 12c). Also, Oruanui glass compositions that are saturated in quartz and plagioclase plot on the high-pressure side of the 200 MPa quartz + plagioclase cotectic on the Qz′–Ab′–Or′ diagram of Blundy & Cashman (2001). These are minimum-pressure estimates because the melts were saturated with a CO_2-bearing gas (Liu *et al.*, 2005) such that $a_{H_2O} < 1$, and experimental studies (e.g. Scaillet & Evans, 1999) show that the effect of reducing a_{H_2O} is to shift the liquidus curves up.

Magmatic H_2O contents have been estimated by two techniques. The method of Housh & Luhr (1991) using plagioclase rim versus glass composition (sample P1209) yields ∼4·6 (An method) and 6·2 (Ab method) wt % at 765°C. Water contents (measured by FTIR) of quartz-hosted melt inclusions from evolved rhyolitic pumices from phases 1, 2, 9 and 10 range between 3·8 and 5·2 wt %, averaging 4·5 wt %, and yield entrapment pressure estimates of 100–200 MPa (Liu *et al.*, 2005). These pressures are lower than suggested from oxide temperatures versus glass CaO compositions (above), and are equivalent to 4–8 km depth for an average Taupo-area crustal density profile (Bibby *et al.*, 1995). Dunbar *et al.* (1989) reported 5·9 wt % H_2O by ion probe for the 29 ka Okaia fall deposit, which is an Oruanui precursor erupted from an area subsequently engulfed by Oruanui caldera collapse.

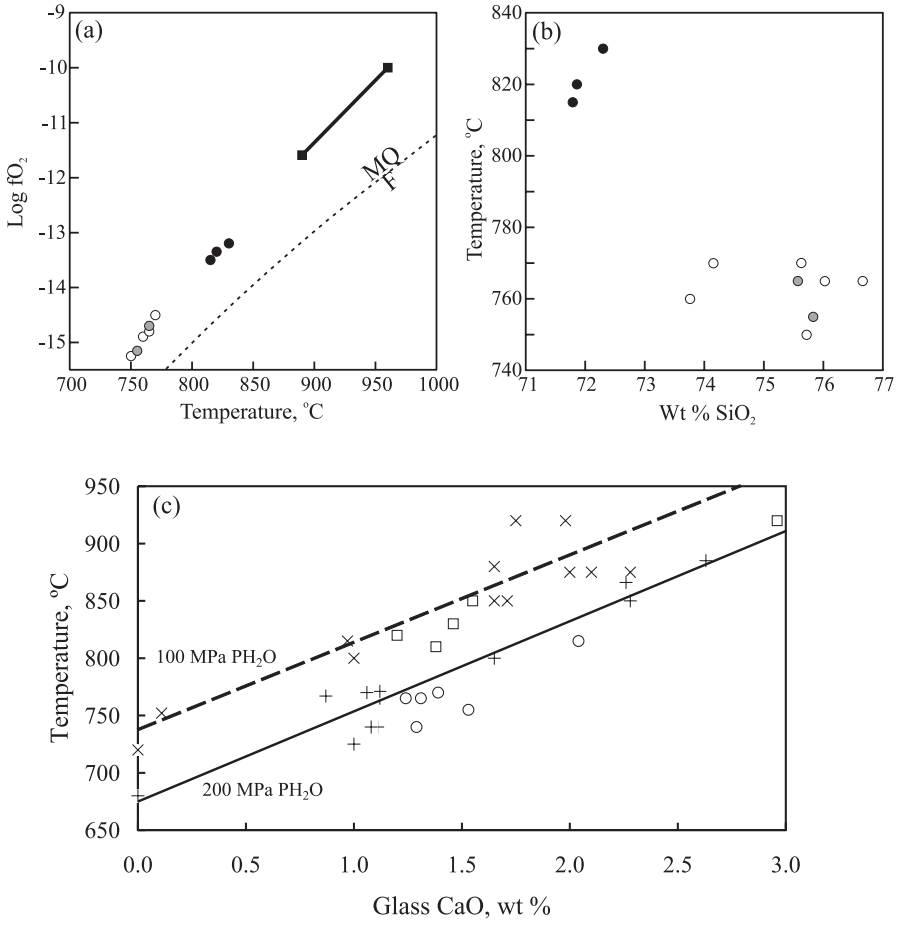

Fig. 12. (a) T–fO_2 plot for Oruanui compositions: evolved (≥73·8 wt % SiO_2) normal rhyolites (open circles), (evolved) high-Mg rhyolites (grey filled circles), less-evolved normal rhyolites (black filled circles) and calc-alkaline mafic clasts (black bar with filled squares at each end represents range in values; see text); FMQ, fayalite–magnetite–quartz buffer. (b) Temperature estimates versus whole-rock wt % SiO_2 for Oruanui rhyolites; symbols as in (a). (c) Plot of Fe–Ti oxide temperature versus CaO content for Oruanui (open circles) and post-Oruanui (open squares) glasses. Straight lines are best-fits to experimentally determined liquidi of silicic glasses with similar K_2O/Na_2O ratios to Taupo rhyolites at $P_{total} = P_{H_2O} =$ 100 (× symbols) and 200 (+ symbols) MPa, compiled from Aramaki (1971), Ui (1971), Piwinskii (1973), Thompson (1983), Grove *et al.* (1997), Cottrell *et al.* (1999), Scaillet & Evans (1999), Coombs & Gardner (2001) and Couch *et al.* (2003). Data from the Qz–Or–Ab system (i.e. CaO = 0, representing the eutectic end-point of fractionation along the liquidus) are from Ebadi & Johannes (1991).

Mafic compositions

Whole-rock compositions

Most mafic clasts have a thin adhering rind of rhyolite and show evidence for small-scale mingling with (or infilling of vesicles by) rhyolite at their margins, but their centres are free of interaction. Removal of any pumiceous contamination during crushing was done to minimize visible contamination of the mafic clasts by host rhyolite. Compositions range from 52 to 63 wt % SiO_2 (Table 5; Electronic Appendix 1), and are divisible into two groups: a higher FeO_t/MgO tholeiitic group and a lower FeO_t/MgO calc-alkaline group that plot almost entirely in the appropriate fields of Miyashiro (1974; Fig. 13a). As well as having higher Fe_2O_3 and TiO_2 for a given SiO_2 content, tholeiitic samples also have higher MnO and Na_2O, lower MgO and CaO, and show strong linear trends in many plots (Fig. 13b–f). Calc-alkaline samples show a more limited range of SiO_2,with poor correlations between SiO_2 and many major elements. Some of the scatter in these plots could be because of the heterogeneous distribution of minerals on the scale of the clasts (typically 5–7 cm across); however, other data (discussed later) imply magma mixing has also occurred.

Of the trace elements analysed by XRF, Rb, Ba, Zr and Y increase uniformly with SiO_2 (Fig. 14), whereas V and Sc (not plotted) uniformly decrease. The tholeiitic samples have higher Sr and lower Cr and Ni than the calc-alkaline samples. Cr and Ni values are widely scattered in the calc-alkaline group and roughly correlate with modal olivine abundances (Sutton, 1995), e.g. P561 has the highest olivine proportion (4%) and the highest Cr (164 ppm) and Ni (43 ppm) contents. Rare earth

Table 5: Analyses of Oruanui mafic clasts

Sample:	P554	P835	P972a	P581	P661	P1514	P742	P651	P574	P575	P942	P919	P409	P584	P986
Group:	tholeiitic	tholeiitic	tholeiitic	tholeiitic	tholeiitic	tholeiitic	tholeiitic	tholeiitic	tholeiitic	tholeiitic	tholeiitic	calc-alkaline	calc-alkaline	calc-alkaline	calc-alkaline
SiO_2	52·27	54·69	56·06	56·52	58·67	59·54	61·07	62·09	62·43	62·93	63·26	56·74	57·40	57·35	57·94
TiO_2	1·44	1·37	1·40	1·68	1·37	1·27	1·12	1·02	1·02	1·05	1·04	0·80	0·80	0·82	0·80
Al_2O_3	16·92	17·82	16·17	17·67	16·61	16·74	17·56	16·10	16·59	16·38	16·01	17·25	17·69	17·80	17·32
Fe_2O_3	12·60	10·44	10·42	9·60	8·22	7·54	6·61	7·03	6·30	6·23	6·12	7·83	7·49	7·50	7·26
MnO	0·19	0·18	0·18	0·18	0·18	0·17	0·16	0·15	0·15	0·16	0·15	0·15	0·15	0·15	0·15
MgO	4·57	3·95	3·55	3·20	2·69	2·59	2·02	2·23	2·03	1·89	1·93	4·45	3·88	4·41	4·01
CaO	8·13	7·15	7·18	5·98	6·28	5·98	5·30	5·45	5·23	5·02	5·09	8·69	8·38	7·71	8·01
Na_2O	3·28	3·53	3·80	4·30	4·24	4·53	4·52	4·15	4·46	4·55	4·51	3·06	3·18	3·26	3·37
K_2O	0·48	0·72	0·79	0·74	1·04	1·07	1·22	1·43	1·40	1·43	1·47	0·83	0·87	0·89	0·94
P_2O_5	0·11	0·15	0·45	0·14	0·69	0·56	0·41	0·35	0·40	0·37	0·42	0·20	0·17	0·11	0·20
(LOI)	1·80	1·89	1·63	2·22	0·94	1·1	1·84	1·61	1·22	1·38	1·50	0·76	1·45	1·37	1·34
(Total)	100·30	99·37	100·34	100·32	99·28	101·58	98·66	98·93	99·36	98·71	99·54	98·57	99·35	99·17	99·44
Rb	11	22	21	19	27	30	40	43	43	43	43	25	28	29	29
Sr	330	324	322	348	335	322	312	287	301	298	291	264	264	263	271
Y	18	18	25	22	30	27	28	26	27	27	29	20	20	19	22
Zr	92	145	126	199	201	203	255	214	229	243	237	145	143	159	166
Nb	4	5	6	7	7	7	8	7	7	8	8	5	4	4	5
Ba	171	244	213	301	275	298	403	345	370	369	371	229	253	280	255
Sc	38	31	32	29	23	25	22	19	19	17	18	29	27	27	26
V	366	218	223	125	99	87	64	111	67	55	53	161	160	143	140
Cr	11	43	19	7	7	6	7	8	8	7	6	97	121	126	88
Co	26	21	34	13	10	9	8	12	9	7	7	23	20	21	20
Ni	5	10	4	2	3	2	3	4	4	2	3	18	18	23	14
Cu	14	11	12	6	5	4	6	6	5	5	5	13	11	11	9
Zn	106	104	94	106	90	93	104	79	80	85	82	73	81	88	74
Ga	20	19	21	20	17	18	18	18	17	17	17	16	17	16	17
La	5·4		11·3	8·5			16·5					9·9			
Ce	14·6		25·0	19·9			37·0					21·6			
Nd	9·50		14·8	11·9			20·9					12·9			
Sm	2·52		3·75	3·08			5·02					3·17			
Eu	1·17		1·41	1·36			1·68					1·26			
Tb	0·59		0·70	0·65			0·84					0·63			
Yb	1·86		2·13	2·13			2·95					2·07			
Lu	0·31		0·36	0·36			0·44					0·35			
Th	1·59		2·65	3·09			5·05					2·65			
U			0·77	0·94			1·40					0·77			
Ta	0·18		0·26	0·41			0·49					0·26			
Hf	2·24		2·99	4·60			5·81					3·43			
Cs	0·66		1·08	0·95			1·76					1·04			
Co	28·7		17·1	9·3			5·8					19·0			
Cr	6		7	5			5					100			
Sc	38·5		29·6	28·5			20·4					30·4			
$^{87}Sr/^{86}Sr$	0·70526	0·70527	0·70534	0·70535	0·70543		0·70540					0·70523			
$^{143}Nd/^{144}Nd$		0·512702					0·512676								
ε_{Nd}		1·25					0·74								

Table 5: continued

Sample:	P931	P650	P560	P562	P929	P561	P546	P951	P987
Group:	calc-alkaline	calc-alkaline	calc-alkaline	calc-alkaline	calc-alkaline	calc-alkaline	calc-alkaline	calc-alkaline	calc-alkaline
SiO_2	58·07	58·05	58·09	58·81	58·77	58·79	59·15	59·81	60·53
TiO_2	0·75	0·89	0·89	0·80	0·75	0·67	0·71	0·87	0·78
Al_2O_3	17·13	18·00	17·90	17·97	17·03	17·02	16·86	16·58	16·61
Fe_2O_3	7·03	7·36	7·35	7·09	6·94	6·79	6·70	6·86	6·53
MnO	0·14	0·16	0·16	0·14	0·14	0·14	0·14	0·15	0·14
MgO	4·16	3·53	3·57	3·77	4·15	5·09	4·45	3·43	3·70
CaO	8·20	7·26	7·24	6·88	7·56	7·15	7·27	7·09	6·59
Na_2O	3·37	3·72	3·78	3·41	3·43	3·14	3·46	3·76	3·67
K_2O	0·95	0·86	0·86	1·01	1·03	1·05	1·08	1·16	1·22
P_2O_5	0·21	0·17	0·16	0·12	0·19	0·16	0·18	0·30	0·22
(LOI)	1·72	1·56	1·58	1·89	1·49	1·54	2·37	1·63	1·46
(Total)	99·65	98·97	99·38	99·23	99·19	99·34	99·75	99·78	99·18
Rb	29	28	28	33	34	36	33	35	38
Sr	268	287	286	257	258	238	252	274	256
Y	22	25	24	21	21	20	21	25	24
Zr	162	215	217	195	169	165	176	179	215
Nb	5	6	6	6	5	5	5	6	6
Ba	263	329	329	377	266	340	282	290	313
Sc	22	29	26	25	22	23	21	22	24
V	133	119	120	123	128	114	113	109	102
Cr	85	74	77	90	99	164	115	60	99
Co	17	18	17	18	20	21	22	15	17
Ni	19	15	15	17	21	43	31	14	23
Cu	12	14	13	11	13	27	8	8	8
Zn	73	105	106	88	74	75	72	74	75
Ga	17	18	18	17	16	16	17	17	16
La		10·2							13·2
Ce		33·1							28·6
Nd		14·0							15·2
Sm		3·68							3·74
Eu		1·36							1·23
Tb		0·72							0·72
Yb		2·56							2·53
Lu		5·05							4·05
U		0·90							1·30
Ta		0·35							0·36
Hf		6·02							4·86
Cs		1·50							1·76
Co		13·6							14·6
Cr		73							108
Sc		27·4							23·4
$^{87}Sr/^{86}Sr$		0·70526							0·70540
$^{143}Nd/^{144}Nd$		0·512676							0·512659
ε_{Nd}		0·74							0·41

Oxide data are normalized to 100% volatile free, but the original LOI values and analytical totals are also given.

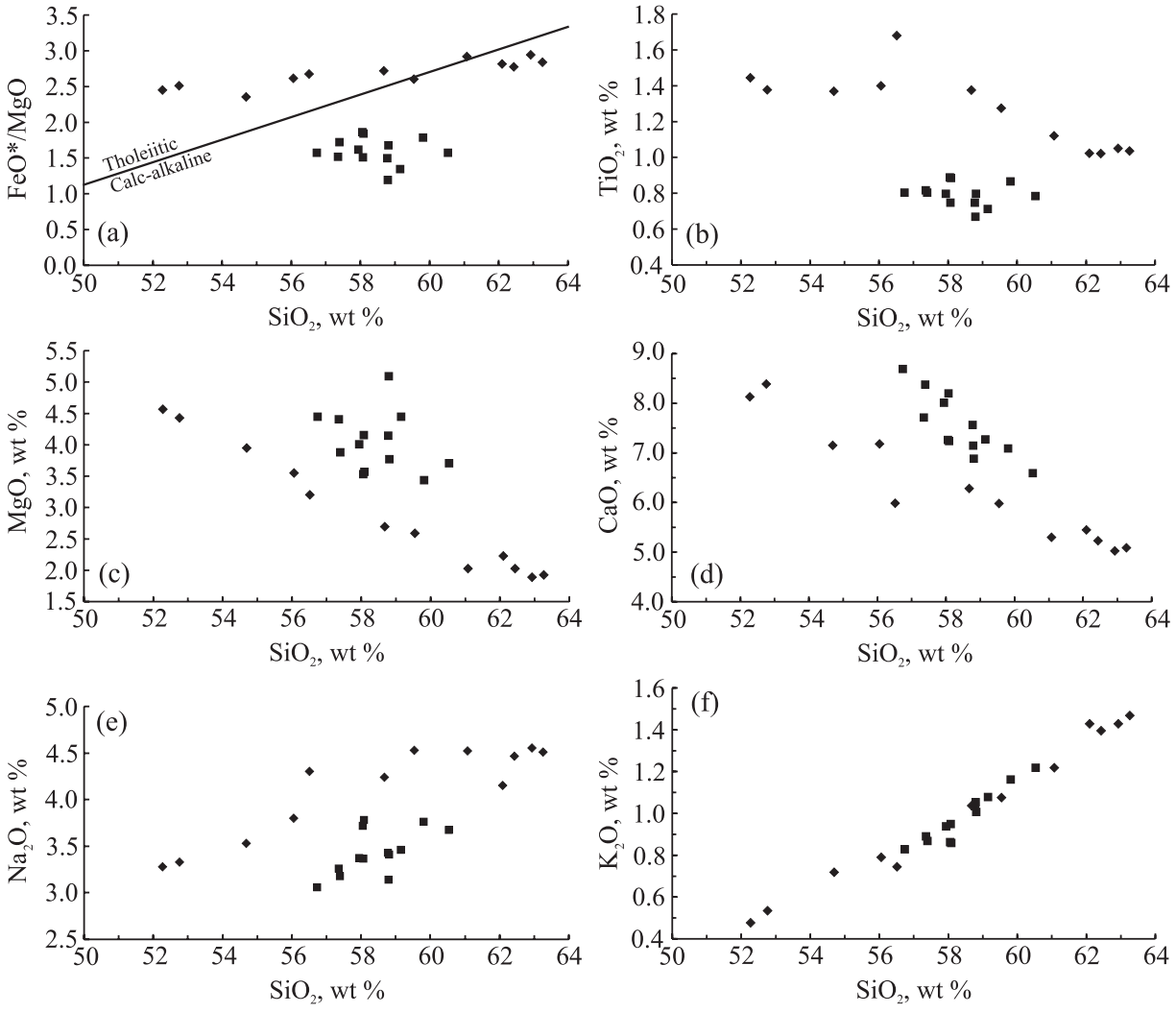

Fig. 13. (a) FeO*/MgO versus SiO_2 plot (after Miyashiro, 1974) for Oruanui mafic clasts (FeO* recalculated from XRF data in Table 5, with adjustment to MgO values to keep total at 100%). (b)–(f) Plots of selected major oxides against silica for Oruanui mafic clasts (Table 5). Filled diamonds are the tholeiitic group and filled squares the calc-alkaline group.

element data (Table 5) are shown in Fig. 7b; no difference is seen between the two groups. The patterns display LREE enrichment ($Ce/Yb_N \sim 2$–3) and fairly flat HREE patterns (~10 × chondrite). The Eu anomaly, calculated as $Eu/Eu^* = Eu_N (Sm_N^2\ Tb_N)^{-1/3}$, ranges from 0·94 to 1·24, with a propagated error of ~3%; this contrasts with other TVZ basalts (Gamble *et al.*, 1993*a*), which have more limited Eu/Eu* values of 0·92–1·06. The ranges of $^{87}Sr/^{86}Sr$ overlap for the two groups; tholeiitic ($n = 6$): 0·70526–0·70543; calc-alkaline ($n = 3$): 0·70523–0·70531 (Table 5), but the tholeiitic samples have higher ε_{Nd} values (Fig. 8). Both groups show increases in $^{87}Sr/^{86}Sr$ with SiO_2 (Fig. 9), suggesting that some mixing with a more radiogenic component has occurred during their evolution.

A notable feature of the Oruanui mafic groups is that neither has compositions that entirely match any comparably mafic suite from the TVZ (Fig. 15). The tholeiitic group has higher Fe_2O_3 and TiO_2 than any other TVZ mafic compositions at a given MgO content (Fig. 15a and b). The nearest match is with the high-$^{87}Sr/^{86}Sr$, high-TiO_2 andesite of the 3·5 ka Unit S (Waimihia) eruption, also from Taupo (Blake *et al.*, 1992: Fig. 15c and d). Although the calc-alkaline samples plot along the same major-element trends as the Ruapehu and White Island composite cones, they have distinctly lower Rb/Zr values (Fig. 15c). Oruanui mafic $^{87}Sr/^{86}Sr$ ratios (Fig. 15c and d) are higher than those of most other central TVZ basalts to andesites, but lie within the ranges of samples from White Island and Ruapehu.

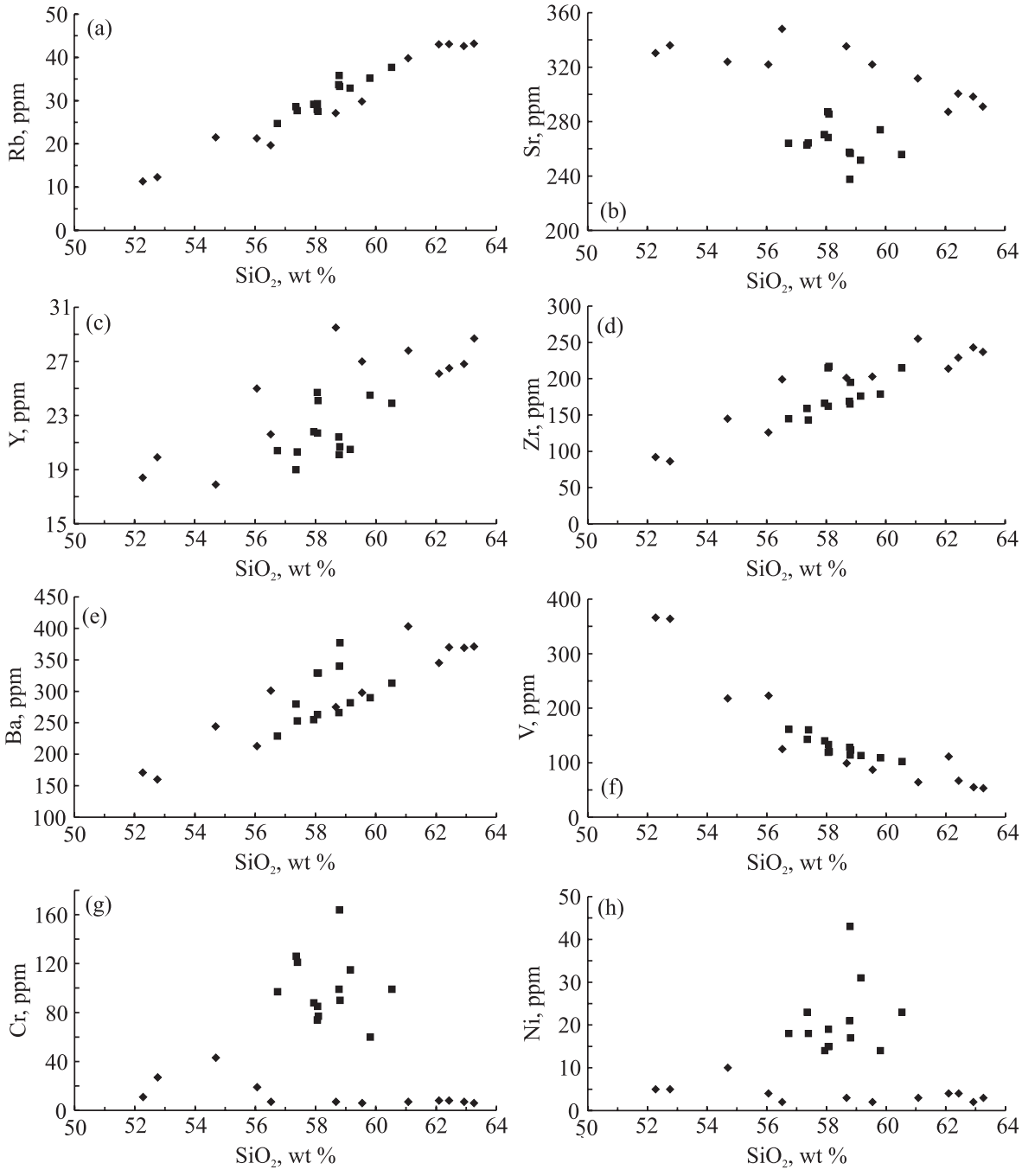

Fig. 14. Plots of selected trace elements against silica for Oruanui mafic clasts (Table 5 for representative data); symbols as in Fig. 13.

Petrography and mineral chemistry

All lapilli to block-sized mafic clasts are phenocryst-poor (<15%), with phenocryst assemblages of plagioclase + clinopyroxene + magnetite ± ilmenite ± olivine ± orthopyroxene ± hornblende (Table 6). The major difference between the tholeiitic and calc-alkaline groups is that olivine occurs only in the latter. Ash-grade mafic fragments are dominantly angular, partly glassy vesicular shards. These shards cannot be allocated to a particular group, except where they have visible olivine present.

Plagioclase is dominant in all samples and forms subhedral to euhedral phenocrysts up to 3 mm long (as well as being the dominant groundmass phase). Crystals often show complex optical zoning, but this is rarely reflected

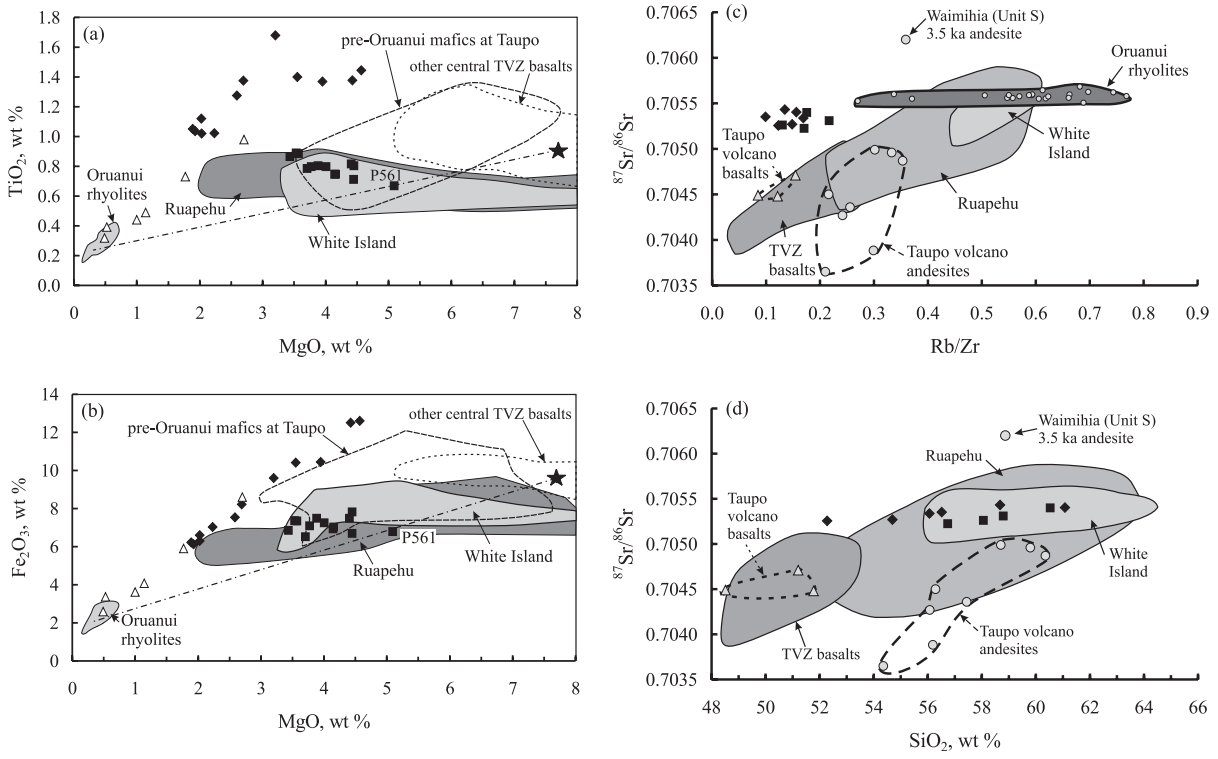

Fig. 15. (a) and (b): compositional data and fields for (a) TiO_2 and (b) total Fe as Fe_2O_3, versus MgO to show the relationships between the Oruanui mafic groups (tholeiitic, filled diamonds; calc-alkaline, filled squares) and other compositions. The Oruanui rhyolite field is from data in Fig. 5. Other fields are pre-Oruanui mafic (basalt and andesite) compositions at Taupo (from Sutton, 1995), other central TVZ basalts (48·5–53·2 wt % SiO_2, from Gamble *et al.*, 1993*a*), and the andesite–dacite composite cones of Ruapehu (Graham & Hackett, 1987) and White Island (Cole *et al.*, 2000) at the southern and northern ends of the TVZ, respectively (Fig. 1). Open triangles represent Oruanui mingled pumices (see also Fig. 17). The star symbol gives the inferred composition of the calc-alkaline primitive end-member (Table 7), as discussed in the text. The dash–dot tie-line connects this primitive end-member to average evolved rhyolite to show the position of the most primitive calc-alkaline mafic sample (P561) along a proposed mixing trend (see text). (c) Plot of $^{87}Sr/^{86}Sr$ versus Rb/Zr for the Oruanui mafic compositions and rhyolites, together with other mafic compositions erupted at Taupo volcano: 'Taupo volcano basalts' (<52 wt % SiO_2) and 'Taupo volcano andesites' (52–63 wt % SiO_2) are pre-Oruanui in age, and the Waimihia (Unit S) andesite is 3·5 ka (data from Sutton, 1995). Comparative fields are for TVZ basalts (Gamble *et al.*, 1993*a*), and andesites to dacites from Ruapehu (Graham & Hackett, 1987) and White Island (Cole *et al.*, 2000). (d) Plot of $^{87}Sr/^{86}Sr$ versus SiO_2, to show comparisons between the Oruanui mafic groups and other mafic to intermediate eruptives from the TVZ; data sources as in (c).

Table 6: Modal phenocryst assemblages of selected Oruanui mafic inclusions, based on counting of 1000 points

Sample	Group	Wt % SiO_2	G'mass	Plag.	Cpx	Opx	Ol	Hb	Opaques	Total phenocrysts
P972a	Th	56·1	93·2	5·0	1·3	0·2	—	0·1	0·2	6·8
P581	Th	56·5	99·0	0·5	0·3	—	—	0·2	(gmass)	1·0
P651	Th	62·1	95·8	2·0	0·5	0·5	—	1·0	0·2	4·2
P919	C-A	56·7	93·8	5·0	1·0	—	0·2	(gmass)	(gmass)	6·2
P560	C-A	58·1	95·0	4·0	0·3	0·2	0·5	(gmass)	(gmass)	5·0
P929	C-A	58·8	91·0	6·7	0·2	0·2	1·8	—	0·1	9·0
P561	C-A	58·8	87·6	6·0	0·2	1·3	4·0	0·8	0·1	12·4
P950	C-A	62·9	89·3	6·0	0·4	0·3	4·0	(gmass)	(gmass)	10·7

Th, tholeiitic; C-A, calc-alkaline.

in strong compositional zoning. Apart from the fact that olivine is found only in the calc-alkaline samples, the most striking difference between the two groups lies in the anorthite contents of plagioclase (see below). In the calc-alkaline clasts, plagioclase shows disequilibrium textures and evidence for two distinctive populations. The first is of often euhedral crystals, with 'dusty' margins suggestive of resorption (Tsuchiyama, 1985).

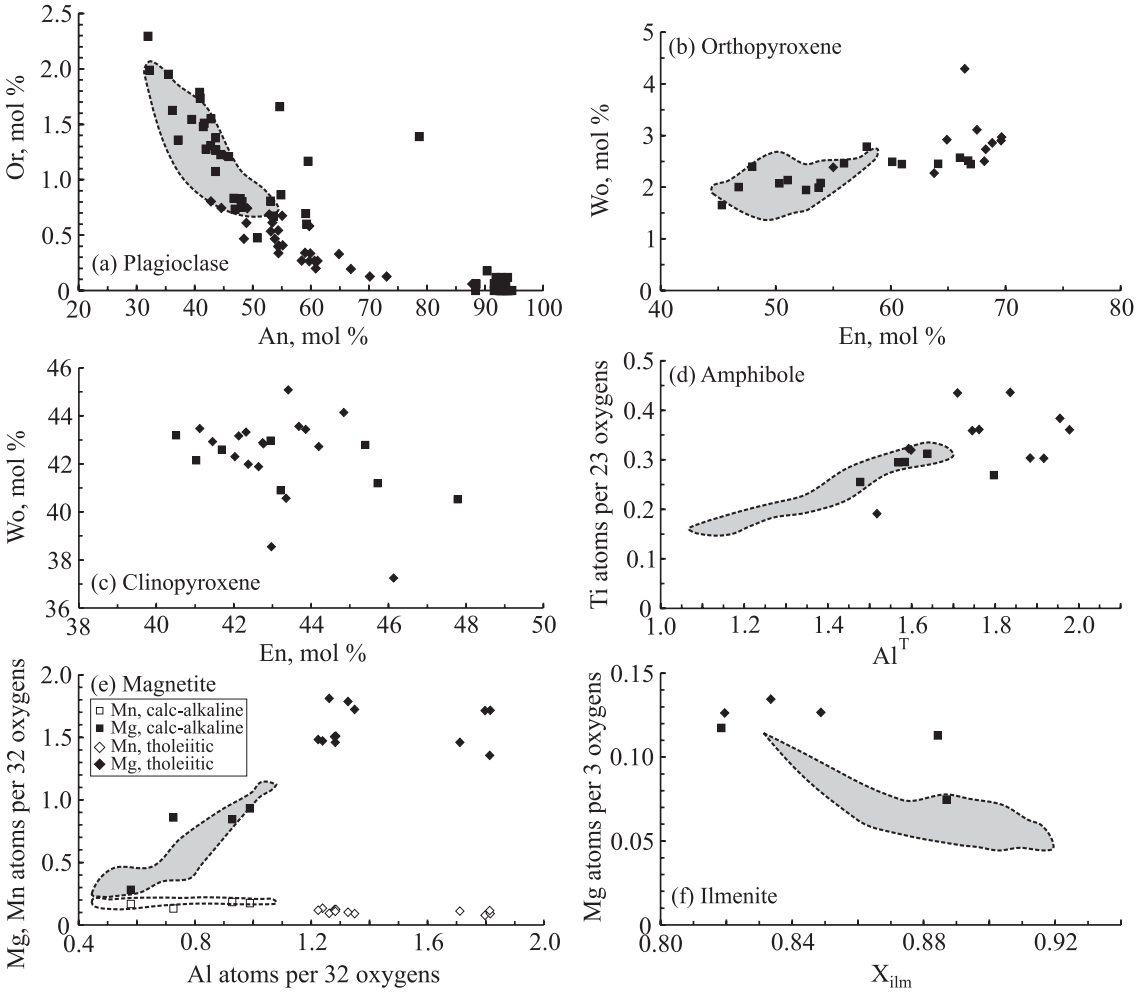

Fig. 16. Summary of mineral compositional data for the Oruanui mafic groups; symbols as in Fig. 13. The shaded fields are those of rhyolitic mineral compositions (from Fig. 10) for comparison (see text).

[Occasionally, thin (~0·01 mm) rims of plagioclase are seen outside these dusty margins, but often evidence for any new growth after resorption is lacking.] The second population is rounded and lacks dusty margins. Clinopyroxene occurs in all samples and orthopyroxene is also present in most, both forming anhedral to euhedral 0·5 mm phenocrysts, with little evidence for zonation. The clinopyroxene to orthopyroxene ratio generally decreases with increasing SiO_2. Olivine, where present, forms large (1–2 mm), often euhedral phenocrysts that show no sign of zonation or resorption. Hornblende occurs in trace quantities in several samples, but is more abundant, as 0·5 mm euhedral crystals, in the two highest-SiO_2 clasts of both calc-alkaline and tholeiitic groups.

The largely finely crystalline groundmasses of the mafic clasts are dominated by plagioclase. Most also contain ~0·1 mm long hornblende and pyroxenes. Fe–Ti oxides, 0·01–0·1 mm in diameter, also occur in the groundmasses, and occasionally as microphenocrysts associated with pyroxenes. Ilmenite has been identified during detailed electron microprobe work on two samples—P561 and P651—but was not found during a similarly detailed search of the more primitive sample P972a.

Compositions of phenocrysts in seven mafic clasts have been analysed by microprobe (full dataset in Electronic Appendix 2); three of tholeiitic: P972a (56·1 wt % SiO_2), P581 (56·5%) and P651 (62·1%), and four of calc-alkaline compositions: P919 (56·7 wt % SiO_2), P560 (58·0%), P929 (58·6%) and P561 (58·6%).

In tholeiitic clasts P972a and P581, plagioclase analyses are scattered in the range $An_{73–43}$ and $Or_{0·13–1·22}$, with one exception—an $An_{87·8}Or_{0·06}$ core found in P972a (Fig. 16a). FeO decreases from 0·75 to 0·25 wt % with decreasing An content. Orthopyroxene compositions cluster in the range $En_{70–64}Wo_{3·2–2·2}$, except for one

crystal of $En_{55}Wo_{2·4}$ (Fig. 16b). Al_2O_3 and TiO_2 contents are scattered, although a subset of analyses have $Al_2O_3/TiO_2 \sim 5$ (Al/Ti $\sim \frac{3}{4}$). Clinopyroxene compositions cluster around a trend extending from $En_{45}Wo_{44}$ to $En_{41}Wo_{43}$ (Fig. 16c). TiO_2 and Al_2O_3 range from 0·45 to 0·95 and 1·7 to 3·6 wt %, respectively. The ratios Ti/Al and En/(En + Fs) show a negative correlation. Amphiboles (Fig. 16d) are tschermakitic; phenocrysts in P651 and groundmass crystals in P581 overlap in composition and have up to $2Al^T$. Magnetite (Fig. 16e) ranges from 26·5 to 38·5% Usp and has 3·3–4·2 wt % MgO and 3·6–5·3% Al_2O_3. Ilmenite (Fig. 16f) is represented by three analyses from P651; these have 82–89% Ilm and 0·07–0·12 Mg atoms per formula unit (3 oxygens).

In calc-alkaline clasts, plagioclase forms two separate populations (Fig. 16a). One has the tight compositional range $An_{88–95}Or_{0–0·2}Ab_{12–5}$ and ~0·4 wt % FeO; these are rounded phenocrysts that lack dusty margins. In contrast, phenocrysts with dusty margins cover a broad range from $An_{60}Or_{0·6}Ab_{40}$ to $An_{32}Or_{2·2}Ab_{66}$ and $0·1 < FeO < 1$ wt %. Two crystals with dusty margins had clear rims that were wide enough to analyse. These rim compositions were $An_{53–55}$, the dusty margins produced $An_{45–55}$ and cores were $An_{40–44}$. Orthopyroxene compositions define a scattered trend between $En_{68}Wo_{2·5}$ and $En_{46}Wo_2$, and have lower TiO_2 and Al_2O_3 contents than orthopyroxene in tholeiitic clasts (Fig. 16b). Crystal zoning is generally not strong, but one crystal had a core of En_{49} and a rim of En_{68}. Clinopyroxene compositions (Fig. 16c) trend from $En_{47·5}Wo_{40·5}$ to $En_{40·5}Wo_{43}$, and have comparable TiO_2 values to but a higher Al_2O_3 range than the tholeiitic group. Amphiboles in the calc-alkaline group are also tschermakitic; Al^T ranges from ~1·5 to 1·8 and compositions overlap those found in tholeiitic clasts (Fig. 16d). Olivine forms a narrow compositional range, with a mean ($n = 15$) of $Fo_{84·8}Fa_{15·2}$ and standard deviation of only 0·24% Fo. Magnetites have 31–35% Usp and Al, Mg and Mn contents that overlap with those found in the rhyolites (Fig. 16e), whereas ilmenites (Fig. 16f) have 82–85% Ilm and ~0·13 Mg atoms per formula unit (3 oxygens).

Intensive parameters

Ilmenite was only found in two samples—P651 (tholeiitic) and P561 (calc-alkaline)—and only in the latter did pairs in Mg/Mn equilibrium occur, yielding temperature estimates of 890°C (log $fO_2 = -11·6$) to 960°C (log $fO_2 = -10·0$) (Fig. 12). Where Fe–Ti oxide geothermometry was not possible, two alternative methods (two-pyroxene and hornblende–plagioclase thermometry) were used in suitable samples. Most estimates cluster at around 950–1050°C, but with wide scatter (Sutton, 1995). No significant differences are seen within or between the tholeiitic and calc-alkaline groups. The abundance of hornblende, along with plagioclase and magnetite in many of the groundmasses of both types of inclusions, is similar to that observed in mafic inclusions in granitoids of the Adamello Massif (Blundy & Sparks, 1992). From crystallization experiments, this assemblage was attributed to overstepping of the nucleation field of olivine and clinopyroxene during rapid quenching to temperatures below 970°C, within the field of hornblende + plagioclase + magnetite.

Mingled pumices

Mingled pumices are exceedingly rare in the Oruanui deposits. Their compositions range between 60·9 and 73·7 wt % SiO_2 and fall along a linear trend consistent with mixing between the most primitive tholeiitic magma and rhyolite of a composition on the boundary between the 'more-' and 'less-evolved' grouping at 73·8 wt % SiO_2 (Figs 15a and 17). Microprobe analyses of crystals in mingled pumice P541 (61·0 wt % SiO_2) revealed rhyolitic plagioclase (An_{43} and An_{33}), rhyolitic and tholeiitic–mafic orthopyroxene ($En_{50}Fs_{48}Wo_2$ and $En_{66}Fs_{31}Wo_3$, respectively), and hornblende with variable compositions but with tholeiitic affinities ($Al^T = 2$; $(Na + K)^A = 0·07$, 0·19 and 0·27; Ti = 0·25, 0·29 and 0·32). The mingled pumices were generated by mechanical mixing between the two end-members, and only limited hybridization has occurred.

ORIGINS OF VARIATIONS IN THE ORUANUI MAGMAS

Rhyolites

Oruanui rhyolite compositions fall along broadly coherent trends (Figs 5 and 6), with no evidence for compositional gaps. However, the data can be interpreted in two contrasting ways.

First, the collinearity of the trends defined by the whole-rock and glass data (Figs 5 and 6) suggests that the bulk compositions of many evolved rhyolites, particularly if the 18 high-Mg rhyolite samples are excluded, could have been generated by crystal fractionation from the higher-temperature less-evolved rhyolites. Note that variations in glass compositions, crystal contents and modes (Tables 2 and 4) preclude an origin for the less-evolved rhyolites by simple crystal accumulation from the more-evolved rhyolites, or vice versa. Derivation of the most-evolved (P888) from the least-evolved rhyolite (P915) by fractionation would require ~28% crystallization, based on the enrichment in Rb and adopting an average $D_{Rb} = 0·03$ (Sutton, 1995). Fractional crystallization along a cotectic involving the phenocryst mineral assemblage, and dominated by plagioclase, can explain the general trends of the major and trace element data seen in Figs 5 and 6 (Sutton, 1995). The change in the apparent

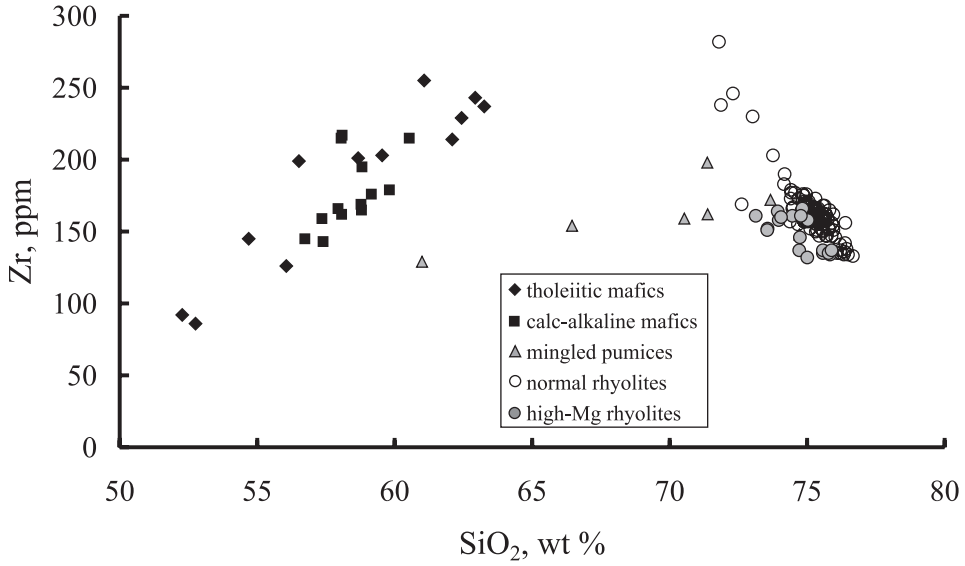

Fig. 17. Plot of Zr versus SiO_2 for all Oruanui samples, to show the relationships between the mafic groups, mingled pumices and the normal and high-Mg rhyolites.

behaviour of Y from weakly compatible to barely compatible (Fig. 6) can be explained by a decrease in the proportion of hornblende in the fractionating assemblage, consistent with its diminishing modal proportion with increasing whole-rock SiO_2.

Secondly, the following features suggest that mixing processes were important in generating the range of compositions recorded.

(1) A single fractional crystallization trend cannot explain all the variability in the rhyolite field, particularly for the high-Mg rhyolite samples which appear to be mixtures. The high-Mg rhyolites are distinctive, for example, when plotted against Zr (Figs 17 and 18a) and Sr; these elements are compatible in the rhyolite but incompatible or marginally compatible in the mafic magmas. The level Zr, higher MgO and inferred lower SiO_2 contents indicate mixing of evolved rhyolite with small amounts of a mafic liquid composition that plots off the right-hand side of Fig. 18a. Using the MgO/FeO_t ratio, the 18 high-Mg rhyolites can be split into subsets of 11 and seven samples (Fig. 18b). Any mixing line between 'normal' rhyolite and tholeiitic mafic compositions does not intercept the compositions of the 11-sample subset, and requires that they include some calc-alkaline material as well. In contrast, the other seven high-Mg rhyolites are similar to the streaky pumices in aligning with the tholeiitic group (Figs 17 and 18b). However, given that the rhyolites, tholeiitic and calc-alkaline mafic components are all compositionally variable, it is not possible to quantify the proportions of the end-members within the high-Mg group any further. Note also that eight of the 11 samples come from a single locality, which also yielded P915, the least-evolved rhyolite. Two of these (P1320B, P1322B; see Electronic Appendix 2) give phenocryst compositions that are unremarkable in comparison with the other rhyolites studied (Figs 10 and 11); however, P1320B yielded trace amounts of clinopyroxene, with En/(En + Fs) and Ti/Al ratios typical of clinopyroxene from tholeiitic rocks.

(2) Values of $^{87}Sr/^{86}Sr$ and ε_{Nd} (Figs 8 and 9) that show scatter beyond that attributable to analytical error.

(3) Phenocryst compositions that do not correlate systematically with whole-rock compositions (Fig. 11). Plagioclase and orthopyroxene from less-evolved normal rhyolites cannot be distinguished compositionally from those in more-evolved normal and high-Mg rhyolites, suggesting that mixing has occurred of crystal populations across the rhyolite spectrum (see Liu *et al.*, 2005). On the other hand, the least-evolved hornblendes, magnetites and ilmenites are found only in the less-evolved rhyolites. The high MgO and Al_2O_3 contents of these magnetites are consistent with the MgO and Al_2O_3 contents of their host rocks, given the correlations found by Shane (1998) in other TVZ tephras. However, mixing is still required to account for the occurrence of low-Mg magnetites throughout the rhyolites.

(4) Zircon U–Th-disequilibrium model-age spectra (Charlier *et al.*, 2005) from Oruanui pumices representative of the dominant rhyolite composition show the presence of young phenocrystic grains and a suite of older grains (~100 ka). The older grains are interpreted to have been remobilized from largely crystallized earlier plutonic bodies.

(5) A minor proportion (1–5%) of the feldspars in the rhyolite have grey cloudy cores with 70–85% An. Sr-isotopic data from these cores imply that they are out

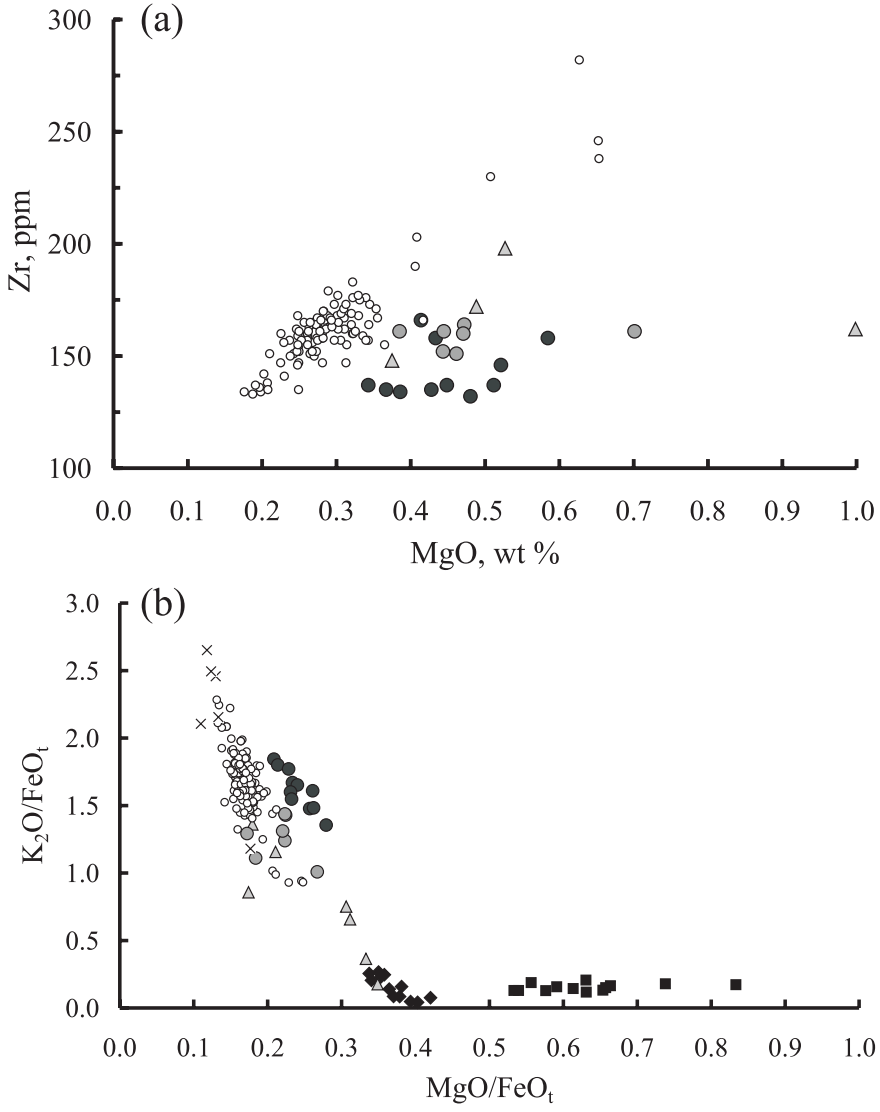

Fig. 18. (a) Plot of normal (open circles) and high-Mg (filled circles) Oruanui rhyolite compositions. Darker filled circles represent 11 high-Mg samples with higher MgO/FeO_t values (see (b)); paler filled circles are the seven other high-Mg samples (see text), and filled triangles are mingled pumices. (b) Plot of all Oruanui compositions to show relationships between the normal rhyolites, high-Mg rhyolites, mingled pumices and mafic compositions; symbols as in (a), with the addition of tholeiitic mafics (filled diamonds), calc-alkaline mafics (filled squares), and glass analyses (crosses). See text for discussion.

of isotopic equilibrium with the host pumice ($^{87}Sr/^{86}Sr$ = 0·70540 in cores; 0·70562 in rims) and represent a xenocrystic component (Charlier *et al.*, 2003*b*).

(6) A minor proportion (four of 62 crystals studied) of the quartz in Oruanui rhyolitic pumices have irregular cores that are dark under CL imaging and contain melt inclusions with Ba-compatible compositional trends that cannot have resulted from fractionation or mixing of a rhyolite with the Oruanui mineral assemblage (Liu *et al.*, 2005).

Thus, although the Oruanui rhyolites and their phenocrysts in large part represent a compositionally coherent suite of crystal-bearing liquids, plausibly related by modest fractionation from P915 (least-evolved) to P888 (most-evolved: Table 2), in detail, mixing processes were important. The mixing is of four main types: (1) mixing of crystals across the rhyolite spectrum (see also Liu *et al.*, 2005); (2) interchange of crystals from mafic liquids comparable in composition to those coerupted with the rhyolites; (3) interchange of minor (quartz, plagioclase) to moderate (zircon) amounts of crystals from pre-existing plutonic rocks; (4) interchange of liquid from mafic sources to generate the shifts in composition in the high-Mg rhyolites.

Mafic compositions

Tholeiitic group

The tholeiitic clasts show coherent whole-rock and mineral compositional trends (e.g. Figs 13–16). These include inflections in TiO_2, P_2O_5 and Y at ~57–58% SiO_2, which is close to where phenocrystic hornblende and ilmenite first appear. This, together with slightly increasing $^{87}Sr/^{86}Sr$ with SiO_2 (Fig. 9a), suggests that fractional crystallization with small amounts of concurrent crustal assimilation are responsible for the compositional variation in this group of magmas. Crustal contamination with Torlesse greywacke has been proposed as important in producing isotopic variability in TVZ basalts (Gamble *et al.*, 1993*a*) and andesites to dacites (Graham & Hackett, 1987; Graham & Cole, 1991; Graham *et al.*, 1995). For example, the involvement of relatively high-Rb/Zr, high-$^{87}Sr/^{86}Sr$ crust in the origin of Ruapehu and White Island magmas is indicated by a positive correlation between $^{87}Sr/^{86}Sr$ and Rb/Zr (Fig. 15c). However, a notable feature of the tholeiitic clasts is that they have high $^{87}Sr/^{86}Sr$ ratios but low Rb/Sr and Rb/Zr ratios such that they plot above the broad AFC trend found in the basalt–andesite–dacite suites of the TVZ. Moreover, they plot above a mixing line between primitive TVZ basalt and bulk Torlesse greywacke, so the primitive tholeiitic clasts require another, unknown contaminant to generate their high $^{87}Sr/^{86}Sr$ ratios. We suggest that the Oruanui tholeiitic magma evolved during stagnation within a crustal region of rhyolite-dominated magmatism, whereas other non-tholeiitic TVZ mafic magmas have either traversed the crust rapidly, with variable degrees of assimilation (monogenetic basalts: Gamble *et al.*, 1993*a*) or have evolved within crustal zones of andesite production (Ruapehu, Edgecumbe, White Island).

Calc-alkaline group

Within the calc-alkaline group, the bimodal plagioclase compositions (Fig. 16a), apparent disequilibrium between some phenocrysts (notably olivine and calcic plagioclase) and whole-rock compositions (Sutton, 1995) imply that mixing was an important genetic process. The composition of the mafic end-member that supplied the olivines (Fo_{85}) and anorthitic plagioclase ($An_{88–95}$) can be constrained using mineral–melt exchange coefficients for hydrous arc basalts determined by Sisson & Grove (1993). Using their olivine–melt Mg–Fe exchange coefficient of 0·28, we calculate a MgO/FeO_t ratio in the melt of ~0·89—a figure matched only by the most magnesian TVZ basalts (e.g. Kakuki: Gamble *et al.*, 1990, 1993*a*). Similarly, the more calcic plagioclase compositions, assuming water saturation, would be in equilibrium with liquids with CaO/Na_2O in the range 4–6—values that again are similar to the most primitive TVZ basalts. Applying Sisson & Grove's (1993) Fe–Mg exchange coefficient for clinopyroxene (0·23) to the liquid's MgO/FeO_t ratio inferred from the olivine composition predicts clinopyroxene with $MgO/FeO_t = 4·9$; however, the most primitive clinopyroxene found in the calc-alkaline rocks has a value of 2·4 that is far too evolved to have been in equilibrium with the mafic end-member. The calc-alkaline primitive end-member is thus inferred to be an olivine–plagioclase basalt, which is consistent with the crystallization sequence of other primitive TVZ basalts (Gamble *et al.*, 1990). This end-member composition can be defined further by noting that the An_{92} crystals contain 0·116 ± 0·017 wt % MgO and that the partition coefficient for MgO between such plagioclase and liquid in Sisson & Grove's (1993) experiments is $D_{MgO} = 0·015$. This gives an approximate MgO content of the liquid in equilibrium with these anorthitic plagioclases of 7·7 wt %. A similar approach using the concentrations and partition coefficients of FeO_t in plagioclase or CaO or Ni in olivine could provide additional constraints but is untenable because these partition coefficients depend on the oxygen fugacity and/or composition of the liquid (Libourel, 1999; Wilke & Behrens, 1999), which parameters are unknown or ill-constrained *a priori*.

The evolved mixing end-member is defined by plagioclase of $An_{40–50}$, and orthopyroxene of ~En_{50} (Fig. 16)—compositions typical of the Oruanui and other rhyolitic magmas at Taupo (Ewart, 1971; Sutton, 1995), although the magma composition in equilibrium with $An_{40–50}$ plagioclase is highly dependent on water content (Sisson & Grove, 1993). However, although mineralogical evidence indicates some role for mixing between a primitive olivine–plagioclase basalt and rhyolite, the calc-alkaline group compositions are scattered and do not plot on a binary mixing line that intercepts the bulk composition of the rhyolites (Figs 15a and b, 17 and 18).

The primitive calc-alkaline end-member, when mixed with the average rhyolite, can plausibly yield the calc-alkaline sample with the highest MgO content (P561; Table 5; Fig. 15a and b). Microprobe analyses showed high-An plagioclase and olivine, together with 'rhyolitic' plagioclase, orthopyroxene, hornblende, magnetite and ilmenite in P561. Assuming that this sample is a mix of average evolved rhyolite (with $SiO_2 > 73·8$ wt %) and primitive magma, then the overall composition of the inferred primitive end-member can be calculated on the basis of a mass balance for MgO (Table 7). The major elements are comparable to those of TVZ basalts, although there is no exact match with any published analysis. The Ca–Na plagioclase–liquid exchange coefficient implied by the calculated end-member ranges from 6·4 to 7·1, consistent with water-rich conditions (Sisson & Grove, 1993). All calc-alkaline samples other than P561 have compositions that are on the tholeiitic side of the rhyolite–P561 mixing line and are therefore three-component mixtures.

Table 7: Calculated composition of the primitive calc-alkaline basalt end-member, based on mass balance constrained by MgO (see text for discussion)

	Evolved average[a]	SD[b]	N[c]	SD%	P561[d]	Calculated end-member[e]
SiO_2	75·29	0·59	112	0·78	58·79	49·84
TiO_2	0·23	0·02	112	8·57	0·67	0·91
Al_2O_3	13·41	0·31	112	2·29	17·02	18·98
Fe_2O_3	1·88	0·17	112	9·15	6·79	9·45
MnO	0·06	0·01	112	9·17	0·14	0·18
MgO	0·28	0·04	112	15·64	5·09	7·70
CaO	1·78	0·12	112	6·77	7·15	10·06
Na_2O	4·16	0·13	112	3·14	3·14	2·59
K_2O	2·87	0·10	112	3·65	1·05	0·06
P_2O_5	0·04	0·01	112	22·01	0·16	0·22
Rb	100	3	110	3·20	36	1
Sr	124·9	7·2	110	5·74	237·6	298·8
Y	23	1	110	2·75	20	19
Zr	160	11	110	6·93	165	168
Nb	6·6	0·4	110	6·24	4·8	3·8
Ba	583	17	110	2·98	340	208
Pb	13	1	109	8·27	6	2
Th	10	1	110	8·74	5	2
U	3	1	110	28·15	0	−1
Sc	4	1	110	25·01	23	33
V	8	3	110	35·66	114	172
Cr	4	1	109	34·88	164	251
Co	2	1	110	36·39	21	31
Ni	3	1	109	49·69	43	65
Cu	3	1	110	48·14	27	40
Zn	41	4	110	8·89	75	94
Ga	13	1	110	6·13	16	18
$^{87}Sr/^{86}Sr$	0·705596	7·7E−05	18	0·011	0·70531	0·70525

[a]Average evolved (>73·8% SiO_2) rhyolite composition from all analyses used in this study. [b]1 SD variation. [c]Number of analyses. [d]Most-primitive erupted calc-alkaline composition based on MgO content (Table 5). [e]Calculated end-member primitive calc-alkaline parental magma, using MgO values.

DISCUSSION

Withdrawal systematics of the Oruanui magmas

If representative Oruanui rhyolite compositional data are plotted in order of eruption (Fig. 19), then it is clear that systematic withdrawal of the range of compositions did not occur. The first-erupted material falls in the compositional range of (and in part defines) the 'dominant' suite of analyses, and examples of the most-evolved and least-evolved rhyolite have not been found in Phase 1 deposits (Fig. 19). The least-evolved samples come from deposits of Phase 3 (along with most of the high-Mg rhyolites) and Phase 6. The most-evolved rhyolite clasts occur in deposits from phases 2, 3 and 10 (Fig. 19). The dominant volume of magma, erupted in Phase 10, includes the most-evolved sample (P888) but lacks the less-evolved compositions. Compositional and thermal variations through deposits erupted in phases 7–10 are negligible. Volatile contents in Oruanui rhyolite melt inclusions suggest that later-erupted material contains higher CO_2 and thus came from greater depth; however, there was no marked gradient in water contents (Liu *et al.*, 2005).

Juvenile mafic compositions do not show systematic variations with stratigraphic position either. Mafic material is present (mostly as ash) to some extent throughout the eruption sequence, very sparsely in phases 1 and 2, then with three spikes in abundance in phases 3 plus 4, 7 and 9 (Wilson, 2001). However, mafic clasts of a size suitable for XRF analysis have been found only in ignimbrite from phases 7 through 10. No systematic variation is present in the ordering or abundance of tholeiitic or calc-alkaline mafic clasts in so far as (1) they are present at all of these levels, (2) both groups are present at localities where multiple hand-specimen sized clasts were found, and (3) the most- and least-evolved examples were collected from comparable stratigraphic levels in the ignimbrite. Available data do not permit us to determine whether the two mafic groups were erupted preferentially during certain eruption phases. However, it seems likely that the time breaks (Table 1) and shifts in vent positions (Fig. 3b) during the eruption can be linked to triggering effects caused by intrusion of the mafic magmas into the main rhyolite magma body.

We infer that the non-systematic tapping of the rhyolite is related to geographic variations in positions of the magma types in the area encompassed by the Oruanui vents. The eruption of less-evolved rhyolite and most of the high-Mg rhyolites in Phase 3 is coincident with a shift in vent positions (Fig. 3b) and the first of the mafic spikes (Wilson, 2001). We additionally infer that the less-evolved normal rhyolite probably did not underlie the whole area of the Oruanui magma body, or was of minor volume because of its apparent absence in deposits of phases 7–10. If appearance of the less-evolved rhyolite and mafic compositions was because of greater depth of drawdown during Phase 3 (Blake & Ivey, 1986; Spera *et al.*, 1986), then they should also both have been recorded during later phases when eruption rates were greater, and substantial amounts of evolved rhyolite had been removed from the chamber. Instead, only the mafic clasts are found. Another notable feature is the spasmodic

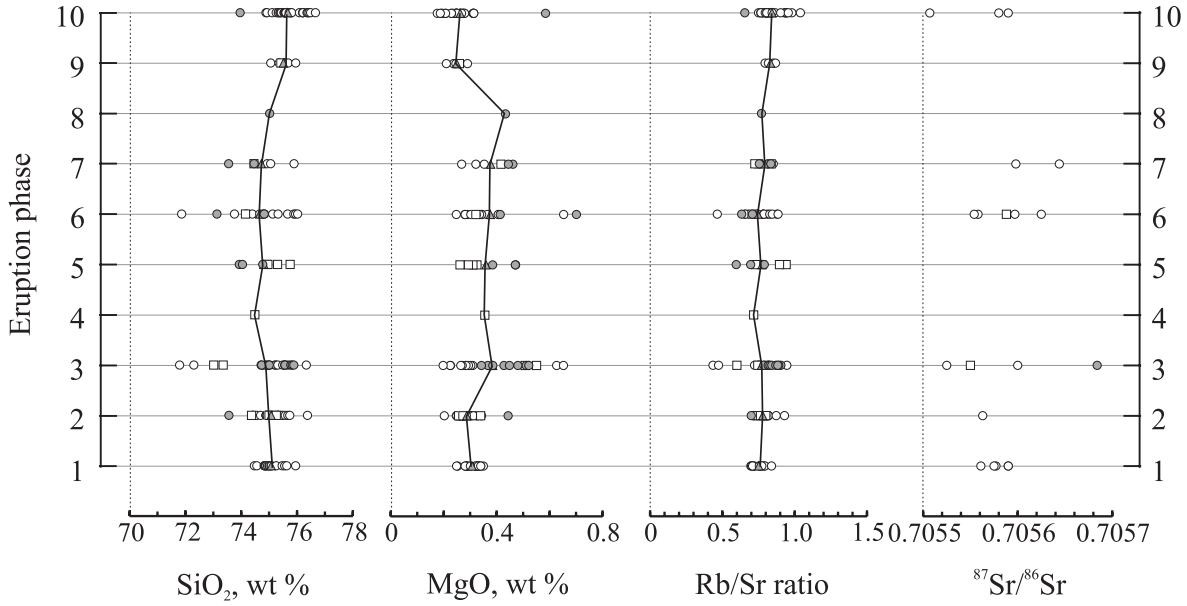

Fig. 19. Selected analytical data from the Oruanui rhyolites versus eruption phase (i.e. stratigraphic level). Open circles represent single clasts; open squares represent multiple clasts (filled symbols are the high-Mg rhyolite samples); the filled triangles (connected by lines) represent arithmetic means of all analyses at each level.

nature of the eruption, with field evidence for time breaks of up to weeks or months (Table 1); however, these had no discernible effects on the magma withdrawal dynamics. Rhyolite compositions do not change much between phases 1 and 2 (Fig. 19) during the longest time break, and yet show significant changes between phases 2 and 3, which overlapped in time but involved a shift in vent positions (Fig. 3b).

The magmatic diversity in the Oruanui eruption occurs in many other silicic systems, but two aspects are unusual here. First, there are the contrasts between the less-evolved normal rhyolites, which are of higher temperature than the evolved rhyolites (Fig. 12), contain some mafic phenocrysts (Fig. 11), but show no geochemical signs of mixing (Fig. 18), versus the high-Mg rhyolites, which were no hotter than the other evolved rhyolites, contain few or no mafic-derived crystals, but show geochemical mixing relationships to one or more mafic compositions. Interactions between mafic and silicic magmas in the Oruanui chamber were complex, and further work is required to disentangle these. Secondly, to have two independent groups of mafic magma each in the 1–2 km^3 range of volumes present simultaneously in such a small geographic area is highly unusual. Parallel pairs of mafic groups are known in close geographic proximity, e.g. 14 km apart in the Havre Trough offshore from the TVZ (Gamble *et al.*, 1993*b*), but are nowhere known to have erupted simultaneously. Again, disentangling the origin and evolutionary pathways of these mafic groups requires further study.

Origin of the Oruanui rhyolites

The origin of the Oruanui rhyolites must be closely linked to general arguments as to the origins and dominance of rhyolite in the central TVZ (e.g. Ewart & Stipp, 1968; Blattner & Reid, 1982; Conrad *et al.*, 1988; McCulloch *et al.*, 1994; Graham *et al.*, 1995). A consensus from the last two papers is that although the isotopic evidence requires a role for some degree of crustal melting, fractionation processes are probably of greater importance. However, modelling based around such inferences is problematic, for three reasons.

(1) The compositional and radiogenic isotopic characteristics of any mafic progenitor are poorly established. Available data on mafic compositions erupted in the central TVZ emphasize their small volume and the lack of a well-constrained compositional trend from which the composition of a single mantle-derived parental magma can be deduced (Gamble *et al.*, 1990, 1993*a*). Thus, a variety of possible mafic compositions can be chosen as the starting point for any AFC processes.

(2) The compositional and radiogenic isotopic characteristics of country-rock assimilants are poorly established. In particular, the recent discovery of U–Pb ages as young as 92 Ma for xenocrystic zircons in post-Oruanui eruptives imply that other materials that are not affiliated with the nearby surficial Torlesse and Waipapa lithologies underlie the Taupo area (Charlier *et al.*, 2005).

(3) In all the papers cited above, a tacit or implicit assumption is that the assimilant is the greywacke metasediments. However, the inference that fractionation is

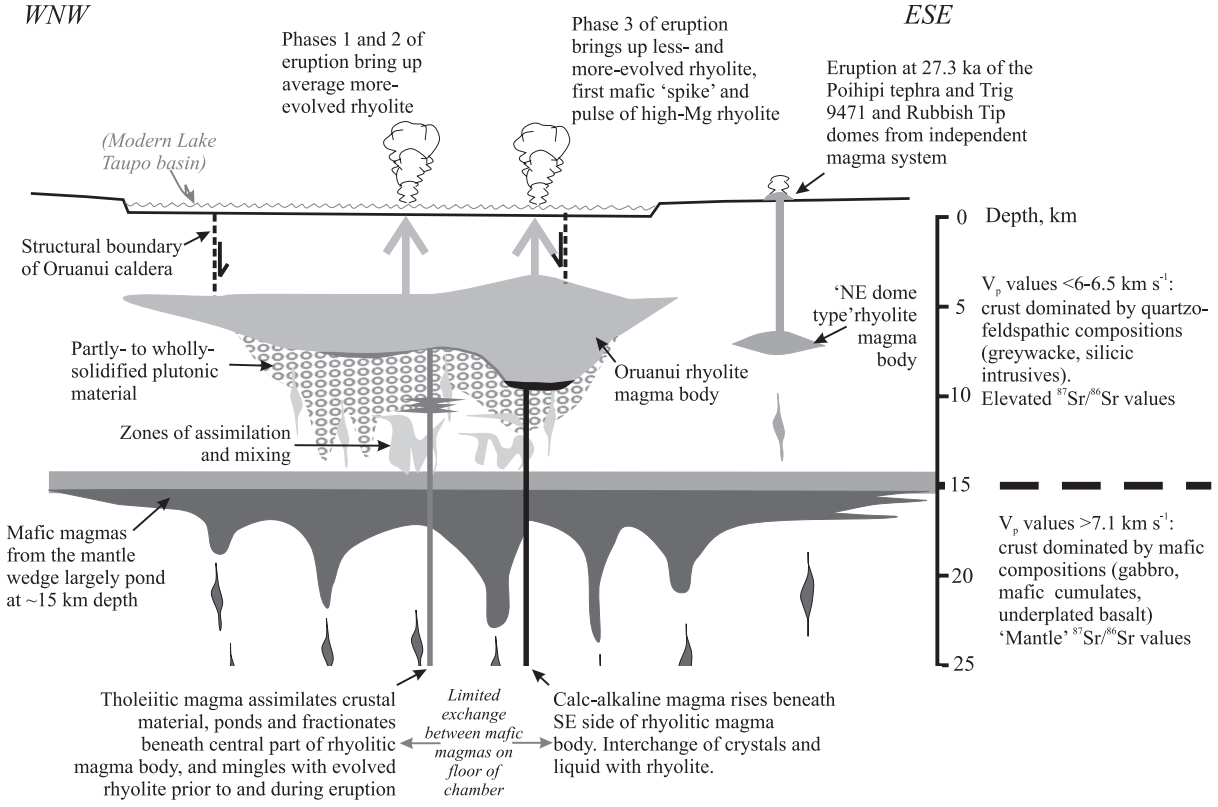

Fig. 20. Scaled schematic cross-section, projected onto a WNW–ESE line, through Taupo volcano to illustrate a crude inferred 2-D layout of the Oruanui magmatic system immediately prior to eruption, and its spatial relationship to the contemporaneous 'NE dome' system that erupted the Poihipi tephra and Trig 9471 and Rubbish Tip domes (Charlier *et al.*, 2005). Vertical and horizontal scales are the same. The crustal section is based on Harrison & White (2004). Vertical and horizontal dimensions of the Oruanui magma body are inferred from volatile data (Liu *et al.*, 2005) and the footprint of the Oruanui structural caldera (Fig. 3), respectively. See text and Charlier *et al.* (2005) for discussion.

important in the generation of TVZ rhyolites inevitably means that large volumes of young plutonic material underlie the central TVZ. Such materials are occasionally sampled as xenoliths (Ewart & Cole, 1967; Brown *et al.*, 1998*b*). Melting or re-mobilization of wholly to partly crystallized plutonic rocks (Charlier *et al.*, 2005) may generate significant volumes of rhyolite that share little direct linkage to their original parentage (e.g. Hildreth, 1981).

Thus, accurate modelling of the chemical–isotopic origins of the Oruanui rhyolites is precluded by the presence of several possible pathways from plausible starting compositions represented by surface metasediments and eruptive rocks. Our data suggest that generation of the spread of compositions in the Oruanui rhyolites involves a suite of processes, among which crystal fractionation from a low-SiO_2 progenitor (taken as being represented by sample P915) is important, provided that crystals have been effectively extracted to form plutonic rocks. Modelling of generation of the Oruanui low-SiO_2 rhyolite progenitor from more-mafic compositions (viz. the most-silicic tholeiitic sample, P742: 61·1 wt % SiO_2) can in turn be demonstrated as feasible (Sutton, 1995), provided that some incorporation of more-radiogenic country-rocks occurs to explain the accompanying increase in $^{87}Sr/^{86}Sr$ ratios (0·70540–0·70553). Ruapehu andesites have interstitial glasses with major and trace-element characteristics that closely resemble those of post-Oruanui rhyolites at Taupo (Price *et al.*, 2005). However, what is not easily explained is how the rhyolitic fractionates could be efficiently extracted, or how such extreme proportions and large volumes of rhyolite can come to be generated in the Taupo area.

The pre-eruptive Oruanui magma body

A reconstruction of the pre-eruptive Oruanui magma body (Fig. 20) is made on the basis of the relationships seen in the rhyolitic and mafic compositions. The following scenario attempts to explain the observations of the magma characteristics, petrogenetic linkages, mode of occurrence (streaky pumice, vesicular enclaves, etc.) and sequence of eruption.

Immediately prior to the eruption, there existed a chamber containing >530 km^3 of rhyolite, mostly of

74–76 wt % SiO_2 and at ~760°C, but with a less-evolved eastern 'root' at higher temperatures (Fig. 12b) and more-evolved rhyolite in some other part(s) of the chamber. The magma contained 3–13% crystals, including small amounts of zircon, quartz and (cloudy cored) plagioclase crystals inherited from an underlying source region that included greywacke with a detrital zircon population as young as 92 Ma and partly to wholly crystallized portions of a young intrusive complex (Charlier *et al.*, 2003*b*, 2005; Liu *et al.*, 2005). The chamber had grown and matured over some 40 kyr prior to the climactic eruption, occasionally venting in small eruptions of Oruanui-type rhyolite. The chamber was crudely discoidal in shape, from the contrast between its vertical extent estimated from studies of volatile components (Liu *et al.*, 2005) and its horizontal 'footprint' constrained by the eruption volume. The chamber roof and floor were not necessarily flat or parallel, and may have contained major roof pendants, cupolas and basins.

Into this chamber was injected primitive tholeiitic basalt, at least as primitive as P554 (Table 5), but already contaminated by interaction with basement lithologies (Fig. 15). This basalt ponded on the chamber floor and continued to assimilate or mingle with more-radiogenic material. Subsequent rapid and sustained heat exchange occurred with the overlying rhyolite because the fluid–fluid interface between the magmas could maintain a very steep thermal gradient and hence high heat fluxes (Huppert & Sparks, 1988). The assimilation undergone by the tholeiitic magma was therefore accompanied by strong cooling that drove fractional crystallization, generating the suite of tholeiitic compositions. Immediately prior to or during the eruption itself, small amounts of this basalt mechanically mixed with the rhyolite, generating streaky pumices (Fig. 17).

Independently, there was injected primitive olivine–plagioclase basalt (Table 7) that flowed across the chamber floor, hybridizing with the rhyolite and generating calc-alkaline compositions similar to P561 (Fig. 15a and b). Possible mechanisms for this mixing are entrainment during vigorous injection of the basalt (Campbell & Turner, 1986; Blake *et al.*, 1992) and convective overturn of the basalt and any rhyolite adhering to the floor of the chamber (Snyder & Tait, 1995). Additional mixing occurred where some of the P561-type hybrid magmas encountered a portion of the tholeiitic magma. Minor contamination of the rhyolite along the upper surface of the mafic magmas led to the spectrum of high-Mg rhyolites (Figs 6 and 17), but there was not enough mafic magma to significantly change the temperature of the high-Mg rhyolite (Fig. 12).

Both mafic magmas must have entered the Oruanui chamber only very shortly before the eruption, on the basis that they were still liquid when ejected. It is probable that injection of the basalts into the rhyolite chamber triggered or primed the Oruanui eruption through some combination of over-pressuring the chamber and weakening of the crust as a result of fault activation accompanying the propagation of the basaltic dykes from depth. Once under way, the eruption would have reduced the pressure in the magma chamber and started to disrupt any stratification in the chamber. Vesiculation within the mafic magmas would have overturned the magmas and helped disrupt the chamber across its full thickness. This explains why mafic spikes, together with most of the spectrum of rhyolite compositions, only appeared well after the eruption sequence had started. Although intrusion of the mafic magmas would have promoted convection in the overlying rhyolite, the diversity of inferred entrapment pressures recorded in quartz crystals in single pumices (i.e. domains 1–10 cm across: Liu *et al.*, 2005) and ages of young crystal growth represented by zircon model-age spectra (Charlier & Zellmer, 2000; Charlier *et al.*, 2005) imply that rhyolite convection was vigorously active prior to mafic intrusion.

Oruanui eruption and models of silicic magmatism

The record presented at Taupo volcano in the products of the Oruanui and other eruptions is in marked contrast to existing models for the rates and recurrence intervals of silicic magmatism. Although discussions about the source and generation rates of the Oruanui magmas depend on chronological information from zircons (Charlier *et al.*, 2005), two generalized points are made here.

Zonation in silicic magma chambers

Zonations in composition–temperature–crystallinity are considered the norm for all substantial bodies of rhyolitic magma (Hildreth, 1981). Whereas the Oruanui rhyolites do show variations in composition (and associated temperature and crystallinity), the majority of samples are from a narrow compositional spectrum which yields model temperatures that realistically are within the errors of the technique (Fig. 12), and has modest variations in crystallinity (Table 4). Compositions down to low-silica rhyolite show no marked increase in crystallinity, and there is simply no evidence for smooth gradients into a significantly more-crystalline root zone. No intermediate hybrids have been found that could imply the presence of a long-lived basal floor of mafic magma to the Oruanui body (see Streck & Grunder, 1999). The high-silica end of the Oruanui rhyolite spectrum shows no evidence for any degrees of trace-element enrichment beyond that which could be attributed to modest amounts of fractionation (28% crystallization from the least- to most-evolved rhyolite), with none of the extreme enrichments or depletions in trace elements characteristic of some high-silica

(>75 wt % SiO_2) rhyolites (e.g. Hildreth, 1981; Mahood, 1981; Streck & Grunder, 1997). The lack of extrema in the Oruanui rhyolites is emphasized by variations in differentiation-sensitive parameters such as the Rb/Sr ratio, which ranges only between 0·43 and 1·04 across the whole range of compositions throughout the entire eruptive sequence (Fig. 19).

Other evidence also counts against there having been any root zone of less-evolved partially liquid intermediate-composition magma beneath the erupted portion of the Oruanui magma body. First, both mafic magma groups are inferred to have intruded and ponded below the rhyolite magma. Both groups would have had densities that would have exceeded any moderately crystal-rich magma of low-silica–rhyolite to dacite composition, and hence would have been expected to have ponded within or below any hypothetical root zone. However, during the eruption, despite significant quantities of mafic material reaching the surface (Wilson, 2001), no trace has been found of any crystal-richer root-zone intermediate eruptives. Similar arguments apply on a smaller scale to the 3·5 ka Unit S (Waimihia) eruption products from Taupo, where a ponded mafic floor to the chamber was also erupted (Blake *et al.*, 1992). Secondly, post-Oruanui activity at Taupo represents a distinct break from the Oruanui and its development. Three crystal-rich dacitic deposits erupted between 21 and 17 ka (Fig. 2) might be interpreted as the rejuvenated products of a partly molten root zone to the Oruanui chamber, but distinct differences in geochemistry and mineralogy (Sutton *et al.*, 2000) and zircon age characteristics (Charlier *et al.*, 2005) rule out such a simple linkage. Rather than having a continuum between a crystal-poor upper portion of material (that was erupted) through increasingly crystal-rich less-evolved compositions to a largely crystalline root zone (e.g. Smith, 1979), we suggest that the Oruanui rhyolite accumulated in a storage chamber that was physically distinct from any underlying zones of partly to wholly crystallized material and hybridized crust, such that the rhyolite was effectively held within a solid-walled container (Charlier *et al.*, 2005). The lack of systematic changes in rhyolite characteristics through the eruption sequence (Fig. 19) and evidence for crystal mixing (previous section and Fig. 11) imply that any systematic minor zonation that might have existed had been disrupted by convection prior to the eruption, with the exception of the basal eastern zone of less-evolved (but still crystal-poor) compositions.

Generation rates of rhyolite magma

Generalized observations and models for the rates of production and eruption of silicic magmas at caldera systems focus around a 'normal' eruption rate of the order 10^{-3} km^3/year, with an associated intrusive rate an order of magnitude higher (Smith, 1979; Crisp, 1984; Shaw, 1985; Jellinek & DePaolo, 2003). In central TVZ, mean eruption rates are an order of magnitude higher than suggested in these models, and the 'intrusion rate' estimated from (assumed steady-state) thermal outputs of geothermal systems is between four and six times greater than the eruption rate (Wilson *et al.*, 1984). At Taupo volcano, the eruption rate over the past ~65 ka has averaged 0·28 m^3/s, with products almost entirely of moderate- to high-silica rhyolite, whereas the present-day 910 MW outputs of geothermal fields within and peripheral to the volcano (Bibby *et al.*, 1995) can be modelled as equivalent to 0·32 m^3/s of intrusive magmatism if steady-state conditions are assumed. Rhyolitic compositions that are interpreted to represent early leaks of the Oruanui magma body go back only to about 65 ka, and zircon model ages are consistent with development of the magma body over about a 40 kyr period (Charlier *et al.*, 2005). The resulting average 0·4 m^3/s rhyolite accumulation rate would demand an extraordinarily high rate of differentiation, but a critical distinction is that we infer, both from the time–space characteristics of silicic compositions (Sutton *et al.*, 1995, 2000) and from zircon model ages (Charlier, 2000; Charlier *et al.*, 2005), that a significant part of the Oruanui magma body represented remobilized, slightly older, partly to wholly crystallized silicic plutonic rocks (by 'silicic' we mean with SiO_2 contents over ~70%, such that crystallization of zircon has occurred; see Fig. 17). We thus infer that whereas the physical assembly of the 530 km^3 of Oruanui magma took place over ~40 kyr, the chemical assembly of the 'Oruanui magma type' or its source plutonic parent(s) must have occurred over a substantially longer period, dating back to at least ~100 ka (Charlier *et al.*, 2005) when the Whakaroa domes (Fig. 3a) were being erupted. The physical assembly of the magma is primarily controlled by the heat influx available for melting and creation of a magma body, whereas the chemical composition of the rhyolite is controlled by the rates of heat loss that must be invoked to accompany differentiation processes. We suggest that during times of elevated heat flux because of mafic intrusion, 'mining' of stockpiled partly to wholly crystallized silicic plutonic rocks can occur to produce bodies of rhyolite at very rapid rates (e.g. ≥0·8 m^3/s prior to the 1·8 ka Taupo eruption: Sutton *et al.*, 2000), well beyond those that could reasonably be achieved by the cooling-driven fractional crystallization of a sufficiently large magma body.

CONCLUSIONS

The 26·5 ka Oruanui eruption had a magma volume of ~530 km^3, ~300 km^3 of which is represented by sampleable extra-caldera rocks. Rhyolite pumice dominates

with minor (<1 wt % overall, but locally ~4 wt %) juvenile mafic (basaltic andesite to high-silica andesite) clasts. Compositional variations across most of the rhyolite eruptives (71·8–76·7 wt % SiO_2, $0{\cdot}43 \leq Rb/Sr \leq 1{\cdot}04$) are superficially consistent with 28% crystal fractionation of the observed mineral phases. However, two forms of mixing also occurred. First, the less-evolved (<73·8 wt % SiO_2) rhyolites exchanged some crystals with a more mafic magma represented by the juvenile mafic clasts, as shown by overlapping crystal compositions in these two suites. Secondly, some evolved (>73·8 wt % SiO_2) rhyolites exchanged liquid (but very few crystals) with magmas of more mafic composition, and have anomalously high MgO contents. Relationships between rhyolite composition and stratigraphic ordering do not show the simple inversion of a systematically zoned chamber. Initial eruptives are neither the most- nor the least-evolved rhyolite erupted, and compositions change more with shifting vent positions than with time during the eruption. The dominant more-evolved rhyolite was mixed by active convection, and not stagnantly stratified.

Mafic clasts form two groups—one tholeiitic, the other calc-alkaline. Variations in the tholeiitic group (52·3–63·3 wt % SiO_2) are attributed to initial assimilation of basement rocks by basaltic magma, followed by a mix of fractionation and further crustal assimilation. Variations in calc-alkaline compositions (56·7–60·5 wt % SiO_2) are because of mixing between a primitive olivine–plagioclase basalt, rhyolite and tholeiitic magmas. Both groups are compositionally distinct from all other TVZ basaltic to andesitic eruptives. The calc-alkaline magma interacted with less-evolved rhyolite under the eastern side of the Oruanui magma chamber, whereas the tholeiitic magma interacted with more-evolved rhyolite farther to the west. Injection of the mafic magmas probably acted as triggers for the eruption, and there was a complex feedback between eruption vigour and the abundance of mafic material ejected.

The Oruanui rhyolite magma body was assembled over ~40 kyr, in part by re-melting of earlier silicic plutonic rocks. It was held prior to eruption in a holding chamber that was physically separated from any crystal-richer root zone. The eruption effectively emptied this holding chamber, reset the Taupo magmatic system, and magmas with Oruanui characteristics (or showing mixing relationships towards Oruanui compositions) have not been produced during the 28 eruptions since, despite overlap in the vent areas. The rapidity with which the Oruanui and younger magma bodies have been assembled and destroyed at Taupo volcano reflects unusually high rates of magma generation and heat transfer—about an order of magnitude greater than considered the norm for silicic magmatism.

ACKNOWLEDGEMENTS

We thank John Watson for analytical support, Hugh Bibby and Martin Reyners for discussions, John Wolff, Martin Streck, Wes Hildreth, Jan Lindsay and Yang Liu for helpful reviews, and Richard Arculus for editorial assistance. We also thank the New Zealand Foundation for Research, Science & Technology (CJNW), the Marsden Fund administered by the Royal Society of New Zealand (CJNW), UK Natural Environment Research Council (BLAC, ANS) and The Open University (BLAC) for financial support.

SUPPLEMENTARY DATA

Supplementary data for this paper are available at *Journal of Petrology* online.

REFERENCES

Aramaki, S. (1971). Hydrothermal determination of the temperature and water pressure of the magma of Aira caldera, Japan. *American Mineralogist* **56**, 1760–1768.

Bacon, C. R. & Hirschmann, M. M. (1988). Mg/Mn partitioning as a test for equilibrium between coexisting Fe–Ti oxides. *American Mineralogist* **73**, 57–61.

Beresford, S. W., Cole, J. W. & Weaver, S. D. (2000). Weak chemical and mineralogical zonation in the Kaingaroa Ignimbrite, Taupo Volcanic Zone, New Zealand. *New Zealand Journal of Geology and Geophysics* **43**, 639–650.

Bibby, H. M., Caldwell, T. G., Davey, F. J. & Webb, T. H. (1995). Geophysical evidence on the structure of the Taupo Volcanic Zone and its hydrothermal circulation. *Journal of Volcanology and Geothermal Research* **68**, 29–58.

Bindeman, I. N. & Valley, J. W. (2003). Rapid generation of both high- and low-$\delta^{18}O$, large-volume silicic magmas at the Timber Mountain/Oasis Valley caldera complex, Nevada. *Geological Society of America Bulletin* **115**, 581–595.

Blake, S. & Ivey, G. N. (1986). Magma-mixing and the dynamics of withdrawal from stratified reservoirs. *Journal of Volcanology and Geothermal Research* **27**, 153–178.

Blake, S., Wilson, C. J. N., Smith, I. E. M. & Walker, G. P. L. (1992). Petrology and dynamics of the Waimihia mixed magma eruption, Taupo Volcano, New Zealand. *Journal of the Geological Society, London* **149**, 193–207.

Blattner, P. & Reid, F. (1982). The origin of lavas and ignimbrites of the Taupo Volcanic Zone, New Zealand, in the light of oxygen isotope data. *Geochimica et Cosmochimica Acta* **46**, 1417–1429.

Blundy, J. & Cashman, K. (2001). Ascent-driven crystallization of dacite magmas at Mount St Helens, 1980–1986. *Contributions to Mineralogy and Petrology* **140**, 631–650.

Blundy, J. D. & Sparks, R. S. J. (1992). Petrogenesis of mafic inclusions in granitoids of the Adamello Massif, Italy. *Journal of Petrology* **33**, 1039–1104.

Briggs, R. M., Gifford, M. G., Moyle, A. R., Taylor, S. R., Norman, M. D., Houghton, B. F. & Wilson, C. J. N. (1993). Geochemical zoning and eruptive mixing in ignimbrites from Mangakino volcano, Taupo Volcanic Zone, New Zealand. *Journal of Volcanology and Geothermal Research* **56**, 175–203.

Brown, S. J. A., Wilson, C. J. N., Cole, J. W. & Wooden, J. (1998*a*). The Whakamaru group ignimbrites, Taupo Volcanic Zone, New Zealand: evidence for reverse tapping of a zoned silicic magma system. *Journal of Volcanology and Geothermal Research* **84**, 1–37.

Brown, S. J. A., Burt, R. M., Cole, J. W., Krippner, S. J. P., Price, R. C. & Cartwright, I. (1998*b*). Plutonic lithics in ignimbrites of Taupo Volcanic Zone, New Zealand: sources and conditions of crystallisation. *Chemical Geology* **148**, 21–41.

Cambray, F. W., Vogel, T. A. & Mills, J. G. (1995). Origin of compositional heterogeneities in tuffs of the Timber Mountain Group: the relationship between magma batches and magma transfer and emplacement in an extensional environment. *Journal of Geophysical Research* **100**, 15793–15805.

Campbell, I. H. & Turner, J. S. (1986). The influence of viscosity on fountains in magma chambers. *Journal of Petrology* **27**, 1–30.

Charlier, B. L. A. (2000). U–Th isotopic constraints on the pre-eruptive dynamics of large-scale silicic volcanism: examples from New Zealand. Ph.D. Thesis, The Open University, Milton Keynes, UK, 393 pp.

Charlier, B. L. A. & Zellmer, G. F. (2000). Some remarks on U–Th mineral ages from igneous rocks with prolonged crystallisation histories. *Earth and Planetary Science Letters* **183**, 457–469.

Charlier, B. L. A., Peate, D. W., Wilson, C. J. N., Lowenstern, J. B., Storey, M. & Brown, S. J. A. (2003*a*). Crystallisation ages in coeval silicic magma bodies: U–Th disequilibrium evidence from the Rotoiti and Earthquake Flat eruption deposits, Taupo Volcanic Zone, New Zealand. *Earth and Planetary Science Letters* **203**, 441–457.

Charlier, B. L. A., Davidson, J. P. & Wilson, C. J. N. (2003*b*). Generation processes in a high-silica rhyolite as recorded in plagioclase crystals from Taupo volcano, New Zealand. Abstracts, EGS–AGU–EUG meeting, Nice, France, 6–11 April 2003. *Geophysical Research Abstracts* **5**, abstract 05352.

Charlier, B. L. A., Wilson, C. J. N., Lowenstern, J. B., Blake, S., van Calsteren, P. W. & Davidson, J. P. (2005). Magma generation at a large, hyperactive silicic volcano (Taupo, New Zealand) revealed by U/Th and U/Pb systematics in zircons. *Journal of Petrology* **46**, 3–32.

Christiansen, R. L. (2001). The Quaternary and Pliocene Yellowstone Plateau Volcanic Field of Wyoming, Idaho, and Montana. *US Geological Survey Professional Paper* **729-G**, 1–143.

Cole, J. W., Thordarson, T. & Burt, R. M. (2000). Magma origin and evolution of White Island (Whakaari) volcano, Bay of Plenty, New Zealand. *Journal of Petrology* **41**, 867–895.

Conrad, W. K., Nicholls, I. A. & Wall, V. J. (1988). Water-saturated and undersaturated melting of metaluminous and peraluminous crustal compositions at 10 kb: evidence for the origin of silicic magmas in the Taupo Volcanic Zone, New Zealand, and other occurrences. *Journal of Petrology* **29**, 765–803.

Coombs, M. L. & Gardner, J. E. (2001). Shallow-storage conditions for the rhyolite of the 1912 eruption at Novarupta, Alaska. *Geology* **29**, 775–778.

Cottrell, E., Gardner, J. E. & Rutherford, M. J. (1999). Petrologic and experimental evidence for the movement and heating of the pre-eruptive Minoan rhyodacite (Santorini, Greece). *Contributions to Mineralogy and Petrology* **135**, 315–331.

Couch, S., Harford, C. L., Sparks, R. S. J. & Carroll, M. R. (2003). Experimental constraints on the conditions of formation of highly calcic plagioclase microlites at the Soufrière Hills Volcano, Montserrat. *Journal of Petrology* **44**, 1455–1475.

Crisp, J. A. (1984). Rates of magma emplacement and volcanic output. *Journal of Volcanology and Geothermal Research* **20**, 177–211.

Davies, G. R. & Halliday, A. N. (1998). Development of the Long Valley rhyolitic magmatic system: strontium and neodymium isotope evidence from glasses and individual phenocrysts. *Geochimica et Cosmochimica Acta* **62**, 3561–3574.

Davies, G. R., Halliday, A. N., Mahood, G. A. & Hall, C. M. (1994). Isotopic constraints on the production rates, crystallisation histories and residence times of pre-caldera silicic magmas, Long Valley, California. *Earth and Planetary Science Letters* **125**, 17–37.

Davy, B. W. & Caldwell, T. G. (1998). Gravity, magnetic and seismic surveys of the caldera complex, Lake Taupo, North Island, New Zealand. *Journal of Volcanology and Geothermal Research* **81**, 69–89.

de Silva, S. L. & Wolff, J. A. (1995). Zoned magma chambers: the influence of magma chamber geometry on sidewall convective fractionation. *Journal of Volcanology and Geothermal Research* **65**, 111–118.

Dunbar, N. W., Hervig, R. L. & Kyle, P. R. (1989). Determination of pre-eruptive H_2O, F and Cl contents of silicic magmas using melt inclusions: examples from Taupo volcanic centre, New Zealand. *Bulletin of Volcanology* **51**, 177–184.

Ebadi, A. & Johannes, W. (1991). Beginning of melting and composition of first melts in the system Qz–Ab–Or–H_2O–CO_2. *Contributions to Mineralogy and Petrology* **106**, 286–295.

Ewart, A. (1971). Notes on the chemistry of ferromagnesian phenocrysts from selected volcanic rocks, Central Volcanic Region. *New Zealand Journal of Geology and Geophysics* **14**, 323–340.

Ewart, A. & Cole, J. W. (1967). Textural and mineralogical significance of the granitic xenoliths from the Central Volcanic Region, North Island, New Zealand. *New Zealand Journal of Geology and Geophysics* **10**, 31–54.

Ewart, A. & Stipp, J. J. (1968). Petrogenesis of the volcanic rocks of the central North Island, New Zealand, as indicated by a study of Sr^{87}/Sr^{86} ratios, and Sr, Rb, K, U and Th abundances. *Geochimica et Cosmochimica Acta* **32**, 699–736.

Ewart, A., Hildreth, W. & Carmichael, I. S. E. (1975). Quaternary acid magma in New Zealand. *Contributions to Mineralogy and Petrology* **51**, 1–27.

Gamble, J. A., Smith, I. E. M., Graham, I. J., Kokelaar, B. P., Cole, J. W., Houghton, B. F. & Wilson, C. J. N. (1990). The petrology, phase relations and tectonic setting of basalts from the Taupo Volcanic Zone, New Zealand and the Kermadec Island Arc–Havre Trough, SW Pacific. *Journal of Volcanology and Geothermal Research* **43**, 253–270.

Gamble, J. A., Smith, I. E. M., McCulloch, M. T., Graham, I. J. & Kokelaar, B. P. (1993*a*). The geochemistry and petrogenesis of basalts from the Taupo Volcanic Zone and Kermadec Island Arc, S.W. Pacific. *Journal of Volcanology and Geothermal Research* **54**, 265–290.

Gamble, J. A., Wright, I. C. & Baker, J. A. (1993*b*). Seafloor geology and petrology in the oceanic to continental transition zone of the Kermadec–Havre–Taupo Volcanic Zone arc system, New Zealand. *New Zealand Journal of Geology and Geophysics* **36**, 417–435.

Ghiorso, M. S. & Sack, R. O. (1991). Fe–Ti oxide geothermometry: thermodynamic formulation and the estimation of intensive variables in silicic magmas. *Contributions to Mineralogy and Petrology* **108**, 485–510.

Graham, I. J. & Hackett, W. R. (1987). Petrology of calc-alkaline lavas from Ruapehu volcano and related vents, Taupo Volcanic Zone, New Zealand. *Journal of Petrology* **28**, 531–567.

Graham, I. J. & Cole, J. W. (1991). Petrogenesis of andesites and dacites of White Island volcano, Bay of Plenty, New Zealand, in the light of new geochemical and isotopic data. *New Zealand Journal of Geology and Geophysics* **34**, 303–315.

Graham, I. J., Cole, J. W., Briggs, R. M., Gamble, J. A. & Smith, I. E. M. (1995). Petrology and petrogenesis of volcanic rocks from the Taupo Volcanic Zone: a review. *Journal of Volcanology and Geothermal Research* **68**, 59–87.

Grove, T. L., Donnelly-Nolan, J. M. & Housh, T. (1997). Magmatic processes that generated the rhyolite of Glass Mountain, Medicine Lake volcano, N. California. *Contributions to Mineralogy and Petrology* **127**, 205–223.

Halliday, A. N., Mahood, G. A., Holden, P., Metz, J. M., Dempster, T. J. & Davidson, J. P. (1989). Evidence for long residence times of rhyolitic magma in the Long Valley magmatic system: the isotopic record in precaldera lavas of Glass Mountain. *Earth and Planetary Science Letters* **94**, 274–290.

Harrison, A. J. & White, R. S. (2004). Crustal structure of the Taupo Volcanic Zone, New Zealand: stretching and igneous intrusion. *Geophysical Research Letters* **31**, L13615, doi: 10.1029/2004GL019885.

Hildreth, W. (1979). The Bishop Tuff: evidence for the origin of compositional zonation in silicic magma chambers. *Geological Society of America Special Paper* **180**, 43–75.

Hildreth, W. (1981). Gradients in silicic magma chambers: implications for lithospheric magmatism. *Journal of Geophysical Research* **86**, 10153–10192.

Hildreth, W., Halliday, A. N. & Christiansen, R. L. (1991). Isotopic and geochemical evidence concerning the genesis and contamination of basaltic and rhyolitic magma beneath the Yellowstone Plateau volcanic field. *Journal of Petrology* **32**, 63–138.

Holland, T. J. & Blundy, J. (1994). Non-ideal interactions in calcic amphiboles and their bearing on amphibole–plagioclase thermometry. *Contributions to Mineralogy and Petrology* **116**, 433–447.

Houghton, B. F., Wilson, C. J. N., McWilliams, M., Lanphere, M. A., Weaver, S. D., Briggs, R. M. & Pringle, M. S. (1995). Chronology and dynamics of a large silicic magmatic system: central Taupo Volcanic Zone, New Zealand. *Geology* **23**, 13–16.

Housh, T. B. & Luhr, J. F. (1991). Plagioclase–melt equilibria in hydrous systems. *American Mineralogist* **76**, 477–492.

Huppert, H. E. & Sparks, R. S. J. (1988). The generation of granitic magmas by intrusion of basalt into continental crust. *Journal of Petrology* **29**, 599–624.

Jellinek, A. M. & DePaolo, D. J. (2003). A model for the origin of large silicic magma chambers: precursors of caldera-forming eruptions. *Bulletin of Volcanology* **65**, 363–381.

Jurado-Chichay, Z. & Walker, G. P. L. (2000). Stratigraphy and dispersal of the Mangaone Subgroup pyroclastic deposits, Okataina Volcanic Centre, New Zealand. *Journal of Volcanology and Geothermal Research* **104**, 319–383.

Leake, B. E.,Woolley, A. R., Arps, C. E. S., Birch, W. D., Gilbert, M. C., Grice, J. D., *et al.* (1997). Nomenclature of amphiboles: Report of the subcommittee on amphiboles of the International Mineralogical Association, Commission on New Minerals and Mineral Names. *American Mineralogist* **82**, 1019–1037.

Leonard, G. S. (2003). The evolution of Maroa Volcanic Centre, Taupo Volcanic Zone, New Zealand. Ph.D. Thesis, University of Canterbury, Christchurch, New Zealand, 322 pp.

Libourel, G. (1999). Systematics of calcium partitioning between olivine and silicate melt: implications for melt structure and calcium content of magmatic olivines. *Contributions to Mineralogy and Petrology* **136**, 63–80.

Liu, Y., Anderson, A. T., Wilson, C. J. N., Davis, A. M. & Steele, R. J. (2005). Pre-eruptive state of the Oruanui rhyolitic magma, Taupo, New Zealand, and comparison with the Bishop magma. *Contributions to Mineralogy and Petrology* (in press).

Mahood, G. A. (1981). Chemical evolution of a Pleistocene rhyolite center—Sierra la Primavera, Jalisco, Mexico. *Contributions to Mineralogy and Petrology* **77**, 129–149.

McCulloch, M. T., Kyser, T. K., Woodhead, J. & Kinsley, L. (1994). Pb–Sr–Nd–O isotopic constraints on the origin of rhyolites from the Taupo Volcanic Zone of New Zealand: evidence for assimilation followed by fractionation from basalt. *Contributions to Mineralogy and Petrology* **115**, 303–312.

Metz, J. M. & Mahood, G. A. (1985). Precursors to the Bishop Tuff eruption: Glass Mountain, Long Valley, California. *Journal of Geophysical Research* **90**, 11121–11126.

Metz, J. M. & Mahood, G. A. (1991). Development of the Long Valley, California, magma chamber recorded in precaldera rhyolite lavas of Glass Mountain. *Contributions to Mineralogy and Petrology* **106**, 379–397.

Mills, J. G., Saltoun, B. W. & Vogel, T. A. (1997). Magma batches in the Timber Mountain magmatic system, southwestern Nevada volcanic field, Nevada, USA. *Journal of Volcanology and Geothermal Research* **78**, 185–208.

Milner, D. M., Cole, J. W. & Wood, C. P. (2003). Mamaku Ignimbrite: a caldera-forming ignimbrite erupted from a compositionally zoned magma chamber in Taupo Volcanic Zone, New Zealand. *Journal of Volcanology and Geothermal Research* **122**, 243–264.

Miyashiro, A. (1974). Volcanic rock series in island arcs and active continental margins. *American Journal of Science* **274**, 321–355.

Nairn, I. A. (2002). Geology of the Okataina Volcanic Centre, scale 1:50,000. Institute of Geological & Nuclear Sciences geological map 25. 1 sheet + 156 pp. Lower Hutt, New Zealand: Institute of Geological & Nuclear Sciences Ltd.

Nairn, I. A., Shane, P. R., Cole, J. W., Leonard, G. J., Self, S. & Pearson, N. (2004). Rhyolite magma processes of the ~AD 1315 Kaharoa eruption episode, Tarawera volcano, New Zealand. *Journal of Volcanology and Geothermal Research* **131**, 265–294.

Newnham, R. M., Eden, D. N., Lowe, D. J. & Hendy, C. H. (2003). Rerewhakaaitu Tephra, a land–sea marker for the Last Termination in New Zealand, with implications for global climate change. *Quaternary Science Reviews* **22**, 289–308.

Piwinskii, A. J. (1973). Experimental studies of igneous rock series, central Sierra Nevada batholith, California: Part II. *Neues Jahrbuch für Mineralogie, Monatshefte* **5**, 193–215.

Potts, P. J., Thorpe, O. W., Isaacs, M. C. & Wright, D. W. (1985). High precision neutron activation analysis of geological samples employing simultaneous counting with both planar and coaxial detectors. *Chemical Geology* **48**, 145–155.

Price, R. C., Gamble, J. A., Smith, I. E. M., Stewart, R. B., Eggins, S. & Wright, I. C. (2005). An integrated model for the temporal evolution of andesites and rhyolites and crustal development in New Zealand's North Island. *Journal of Volcanology and Geothermal Research* **140**, 1–24.

Ramsey, M. H., Potts, P. J., Webb, P. C., Watkins, P., Watson, J. S. & Coles, B. J. (1995). An objective assessment of analytical method precision: comparison of ICP-AES and XRF for the analysis of silicate rocks. *Chemical Geology*, **124**, 1–19.

Scaillet, B. & Evans, B. W. (1999). The 15 June 1991 eruption of Mount Pinatubo: I—Phase equilibria and pre-eruption P–T–fO_2–fH_2O conditions of the dacite magma. *Journal of Petrology* **40**, 381–411.

Self, S. & Sparks, R. S. J. (1978). Characteristics of widespread phreatomagmatic ashes generated by the interaction of silicic magma and water. *Bulletin Volcanologique* **41**, 196–212.

Shane, P. (1998). Correlation of rhyolitic pyroclastic eruptive units from the Taupo volcanic zone by Fe–Ti oxide compositional data. *Bulletin of Volcanology* **60**, 224–238.

Shaw, H. R. (1985). Links between magma–tectonic rate balances, plutonism, and volcanism. *Journal of Geophysical Research* **90**, 11275–11288.

Sisson, T. W. & Grove, T. L. (1993). Experimental investigations of the role of H_2O in calc-alkaline differentiation and subduction zone magmatism. *Contributions to Mineralogy and Petrology* **113**, 143–166.

Smith, R. L. (1979). Ash-flow magmatism. *Geological Society of America Special Paper* **180**, 5–27.

Snyder, D. & Tait, S. (1995). Replenishment of magma chambers: comparison of fluid-mechanic experiments with field relations. *Contributions to Mineralogy and Petrology* **122**, 230–240.

Spera, F. J. & Crisp, J. A. (1981). Eruption volume, periodicity and caldera area: relationships and interferences on development of compositional zonation in silicic magma chambers. *Journal of Volcanology and Geothermal Research* **11**, 169–187.

Spera, F. J., Yuen, D. A., Greer, J. C. & Sewell, G. (1986). Dynamics of magma withdrawal from stratified magma chambers. *Geology* **14**, 723–726.

Stix, J., Goff, F., Gorton, M. P., Heiken, G. & Garcia, S. R. (1988). Restoration of compositional zonation in the Bandelier silicic magma chamber between two caldera-forming eruptions: geochemistry and origin of the Cerro Toledo Rhyolite, Jemez Mountains, New Mexico. *Journal of Geophysical Research* **93**, 6129–6147.

Streck, M. L. & Grunder, A. L. (1997). Compositional gradients and gaps in high-silica rhyolites of the Rattlesnake Tuff, Oregon. *Journal of Petrology* **38**, 133–163.

Streck, M. J. & Grunder, A. (1999). Enrichment of basalt and mixing of dacite in the root zone of a large rhyolite magma chamber: inclusions and pumices from the Rattlesnake Tuff, Oregon. *Contributions to Mineralogy and Petrology* **136**, 193–212.

Sun, S.-s. & McDonough, W. F. (1989). Chemical and isotopic systematics of oceanic basalts: implications for mantle composition and process. In: Saunders, A. D. & Norry, M. J. (eds) *Magmatism in the Ocean Basins*. *Geological Society, London, Special Publications* **42**, 313–345.

Sutton, A. N. (1995). Evolution of a large silicic magma system: Taupo volcanic centre, New Zealand. Ph.D. Thesis, The Open University, Milton Keynes, UK, 416 pp.

Sutton, A. N., Blake, S. & Wilson, C. J. N. (1995). An outline geochemistry of rhyolite eruptives from Taupo volcanic centre, New Zealand. *Journal of Volcanology and Geothermal Research* **68**, 153–175.

Sutton, A. N., Blake, S., Wilson, C. J. N. & Charlier, B. L. A. (2000). Late Quaternary evolution of a hyperactive rhyolite magmatic system: Taupo volcanic centre, New Zealand. *Journal of the Geological Society, London* **157**, 537–552.

Thompson, R. N. (1983). Thermal aspects of the origin of Hebridean Tertiary acid magmas: II—Experimental melting behaviour of the granites at 1 kbar P_{H2O}. *Mineralogical Magazine* **47**, 111–121.

Tsuchiyama, A. (1985). Dissolution kinetics of plagioclase in the melt of the system diopside–albite–anorthite, and origin of dusty plagioclase in andesites. *Contributions to Mineralogy and Petrology* **89**, 1–16.

Ui, T. (1971). Genesis of magma and structure of magma chamber of several pyroclastic flows in Japan. *Journal of the Faculty of Science, University of Tokyo, II* **18**, 53–127.

Vogel, T. A., Noble, D. C. & Younker, L. W. (1989). Evolution of a chemically zoned magma body: Black Mountain volcanic center, southwestern Nevada. *Journal of Geophysical Research* **94**, 6041–6058.

Vucetich, C. G. & Howorth, R. (1976). Late Pleistocene tephrostratigraphy in the Taupo District, New Zealand. *New Zealand Journal of Geology and Geophysics* **19**, 51–69.

Watson, E. B. & Harrison, T. M. (1983). Zircon saturation revisited: temperature and composition effects in a variety of crustal magma types. *Earth and Planetary Science Letters* **64**, 295–304.

Wilke, M. & Behrens, H. (1999). The dependence of the partitioning of iron and europium between plagioclase and hydrous melt on oxygen fugacity. *Contributions to Mineralogy and Petrology* **137**, 102–114.

Wilson, C. J. N. (1993). Stratigraphy, chronology, styles and dynamics of late Quaternary eruptions from Taupo volcano, New Zealand. *Philosophical Transactions of the Royal Society of London* **A343**, 205–306.

Wilson, C. J. N. (2001). The 26·5 ka Oruanui eruption, New Zealand: an introduction and overview. *Journal of Volcanology and Geothermal Research* **112**, 133–174.

Wilson, C. J. N., Rogan, A. M., Smith, I. E. M., Northey, D. J., Nairn, I. A. & Houghton, B. F. (1984). Caldera volcanoes of the Taupo Volcanic Zone, New Zealand. *Journal of Geophysical Research* **89**, 8463–8484.

Wilson, C. J. N., Houghton, B. F. & Lloyd, E. F. (1986). Volcanic history and evolution of the Maroa–Taupo area, central North Island. In: Smith, I. E. M. (ed.) *Late Cenozoic Volcanism in New Zealand. Royal Society of New Zealand Bulletin* **23**, 194–223.

Wilson, C. J. N., Houghton, B. F., McWilliams, M. O., Lanphere, M. A., Weaver, S. D. & Briggs, R. M. (1995). Volcanic and structural evolution of Taupo Volcanic Zone, New Zealand: a review. *Journal of Volcanology and Geothermal Research* **68**, 1–28.

Wolff, J. A. (1985). The effect of explosive eruption processes on geochemical patterns within pyroclastic deposits. *Journal of Volcanology and Geothermal Research* **26**, 189–201.